Supplementary Information

Tracking four-dimensional atomic evolution of single nanocatalysts throughout the life cycles

Jisheng Xie, Zhiheng Xie, Dijin Jiang, Shiyun Li, Yiheng Dai, Yao Zhang, Mufan Li[†], Jihan Zhou[†]

Beijing National Laboratory for Molecular Sciences, Center for Integrated Spectroscopy, College of Chemistry and Molecular Engineering, Peking University, Beijing, 100871, China.

[†] Correspondence and requests for materials should be addressed to M. L. (email: mufanli@pku.edu.cn) and J. Z. (email: jhzhou@pku.edu.cn)

This PDF file includes Supplementary Tables 1-4, Supplementary Figs. 1-30 and captions for Supplementary Movies 1-5.

Other Supplementary Materials for this manuscript include Supplementary Movies 1-5.

Supplementary Table 1 | Volumes of inks used in sample preparation

Name of particle series	Particle-1	Particle-2	Particle-3
Pd@Pt/CNT ink (μL)	1	2	1

Supplementary Table 2 | AET data and analysis

Particle name	Particle-1			Particle-2		Particle-3	
	NP_{1_0}	$NP_{1\_0.5K}$	$NP_{1\_1.5K}$	NP_{2_0}	$NP_{2\_0.1K}$	NP_{3_0}	$NP_{3\_2.5K}$
Data collection*							
Tilt range (°)	-72° 72.5°	-69° 75.5°	-72° 75°	-72° 70°	-72° -70°	-72° 72.5°	-72° 71°
Electron dose (10^5 e^- $Å^{-2}$)	3.0	2.8	2.5	2.9	2.9	3.0	2.9
Refinement†							
R (%)‡	6.8	6.4	8.7	5.2	4.9	5.6	6.9
Statistics of atoms							
Number of Pd	10353	10373	5222	14331	14405	13339	7930
Number of Pt	2205	2163	1475	2641	2588	2284	985
Common positions							
Number of positions	12108	12108/6172§	6172	16634	16634	/#	/#
Ratio to total (%)	96.4	96.6/49.2§	92.2	98.0	97.8	/#	/#
Consistent atoms							
Number of Pd	9423	9423/4569¶	4569	13407	13407	/#	/#
Number of Pt	1405	1405/251¶	251	1925	1925	/#	/#
Ratio to total (%)	89.4	89.4/78.1¶	78.1	92.2	92.2	/#	/#

* Operation parameters of datasets are: 300 kV voltage, 25 mrad convergence semi-angle, 40.6 mrad HAADF detector inner semi-angle and 200 mrad HAADF detector outer semi-angle, the pixel size is 0.352 Å.

† Real space iterative reconstruction (RESIRE) algorithm[1] was used to reconstruct each experimental tilt series, with oversampling ratio being 4 and number of iterations being 300.

‡ A R-factor is used to calculate the difference between calculated and measured projections[1].

§ 12108 and 96.6% are the common atoms and ratio to total atoms between $Pd@Pt_{1\_0}$ and $Pd@Pt_{1\_0.5K}$; and 6172 and 49.2% are the consistent atoms and ratio to common positions between $Pd@Pt_{1\_0.5K}$ and $Pd@Pt_{1\_1.5K}$, respectively.

¶ 9423, 1405 and 89.4% are the consistent atoms and ratio to total atoms between $Pd@Pt_{1\_0}$ and $Pd@Pt_{1\_0.5K}$; and 4569, 251 and 78.1% are the consistent atoms and ratio to common positions between $Pd@Pt_{1\_0.5K}$ and $Pd@Pt_{1\_1.5K}$, respectively.

\# For Particle-3, due to the drastic changes between $Pd@Pt_{3\_0}$ and $Pd@Pt_{3\_2.5K}$, it is hard to find the common positions of the two structures for further analysis.

Supplementary Table 3 | The delta values of CSROPs (ΔCSROPs) between datasets

Orientations	Particle-1		Particle-2	Particle-3
	$\Delta CSROP_{0.5K - 0}$*	$\Delta CSROP_{1.5K - 0.5K}$†	$\Delta CSROP_{0.1K - 0}$‡	$\Delta CSROP_{2.5K - 0}$§
{100}-1¶	-0.03	0.62#	-0.01	-0.43
{100}-2	0.01	-0.01	-0.10	-1.1
{100}-3	0.19	0.18	-0.12	-0.37
{100}-4	-0.16	-0.02	-0.13	-0.61
{100}-5	0.02	-0.06	0.08	0.19
{100}-6	0.01	-0.02	0.09	-1.62
{111}-1	-0.11	0.55	-0.14	0.09
{111}-2	0.12	0.47	0.05	0.67
{111}-3	0.15	0.30	-0.17	0.36
{111}-4	-0.03	0.73	0.10	0.03
{111}-5	0.07	-0.22#	0.04	0.08
{111}-6	-0.05	0.61	0.19	-0.38
{111}-7	-0.10	0.02	-0.09	-0.13
{111}-8	0.27	0.27	-0.16	0.20

* $\Delta CSROP_{0.5K - 0}$ means the delta values of averaged CSROPs between $Pd@Pt_{1\_0.5K}$ and $Pd@Pt_{1\_0}$.

† $\Delta CSROP_{1.5K - 0.5K}$ means the delta values of averaged CSROPs between $Pd@Pt_{1\_1.5K}$ and $Pd@Pt_{1\_0.5K}$.

‡ $\Delta CSROP_{0.1K - 0}$ means the delta values of averaged CSROPs between $Pd@Pt_{2\_0.1K}$ and $Pd@Pt_{2\_0}$.

§ $\Delta CSROP_{2.5K - 0}$ means the delta values of averaged CSROPs between $Pd@Pt_{3\_2.5K}$ and $Pd@Pt_{3\_0}$.

¶ The assigned numbers for {100} or {111} orientations are shown in Fig. 3e and Supplementary Figs. 29e and 30e.

While the delta values in particle-2 are all smaller than 0.20, indicating little changes during the 100 cycles. The delta values higher than 0.2 or lower than -0.2 in the table are highlighted in red or green, respectively.

Supplementary Table 4 | XAFS fitting parameters for Pd@Pt at Pt L_3-edge

Sample	CN*	R (Å)†	σ^2 (Å^2)‡	ΔE_0 (eV)§	R-factor^e
Pt foil	12.0¶	2.76±0.001	0.0045±0.0002	8.49±0.36	0.002
Pristine	5.0±0.5	2.74±0.009	0.0048±0.0012	4.88±0.85	0.005
After 0.6 V_{RHE}	6.3±0.5	2.73±0.009	0.0053±0.0009	5.15±0.85	0.004
After 0.9 V_{RHE}	9.2±1.0	2.74±0.008	0.0050±0.0011	6.50±0.83	0.020

- S_0^2 (amplitude reduction factor) was set to be 0.79.

* Coordination number for the corresponding shell.

† Interatomic distance

‡ Debye-Waller factors.

§ Edge-energy shift; e: Goodness of fitting.

¶ This value was fixed during fitting, based on the known structure of Pt metal.

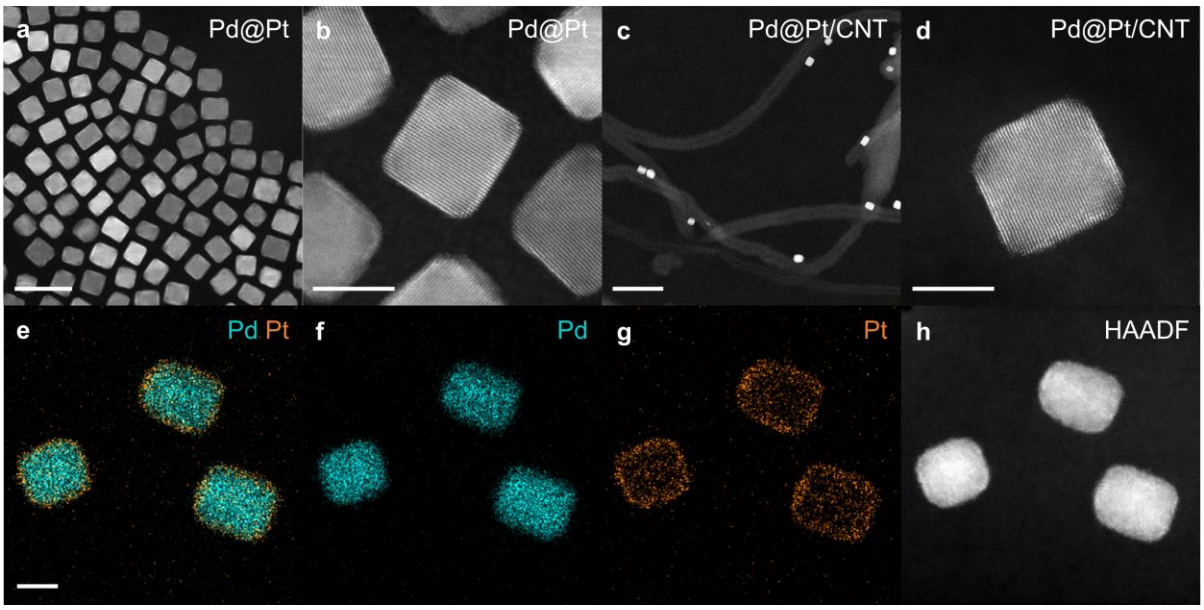

Supplementary Fig. 1 | Characterization of Pd@Pt NPs and Pd@Pt/CNT nanocatalysts. **a, b,** ADF-STEM images of Pd@Pt NPs at low **(a)** and high **(b)** magnifications. Scale bars are 20 nm and 5 nm in **(a)** and **(b)**, respectively. **c, d,** ADF-STEM images of Pd@Pt/CNT nanocatalysts at low **(c)** and high **(d)** magnifications. Scale bars are 50 nm and 5 nm in **(c)** and **(d)**, respectively. **e-h,** EDS mapping of Pd@Pt/CNT NPs: images of merged Pd and Pt signals **(e)**, Pd **(f)**, Pt **(g)** and ADF signals **(h)**. Scale bars are 5nm for **(e-h)**. Both Pd@Pt NPs and Pd@Pt/CNT exhibit a cuboctahedral morphology and are highly uniform.

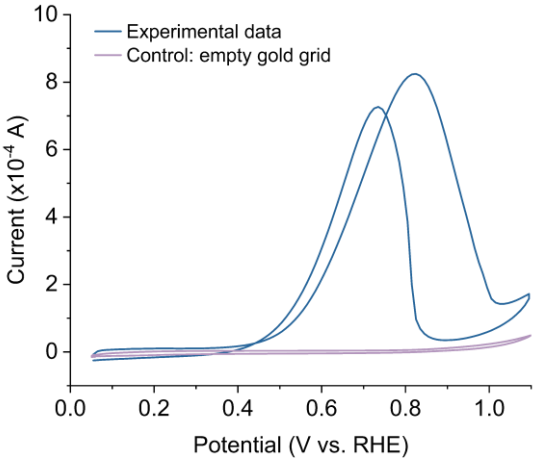

Supplementary Fig. 2 | CV curves tested with a prepared sample and an empty gold grid. While the experimental data shows a typical electrochemical curve of electrocatalytic ethanol oxidation reaction, the curve tested on an empty gold grid without any catalyst shows no reaction activity towards the working condition in this study.

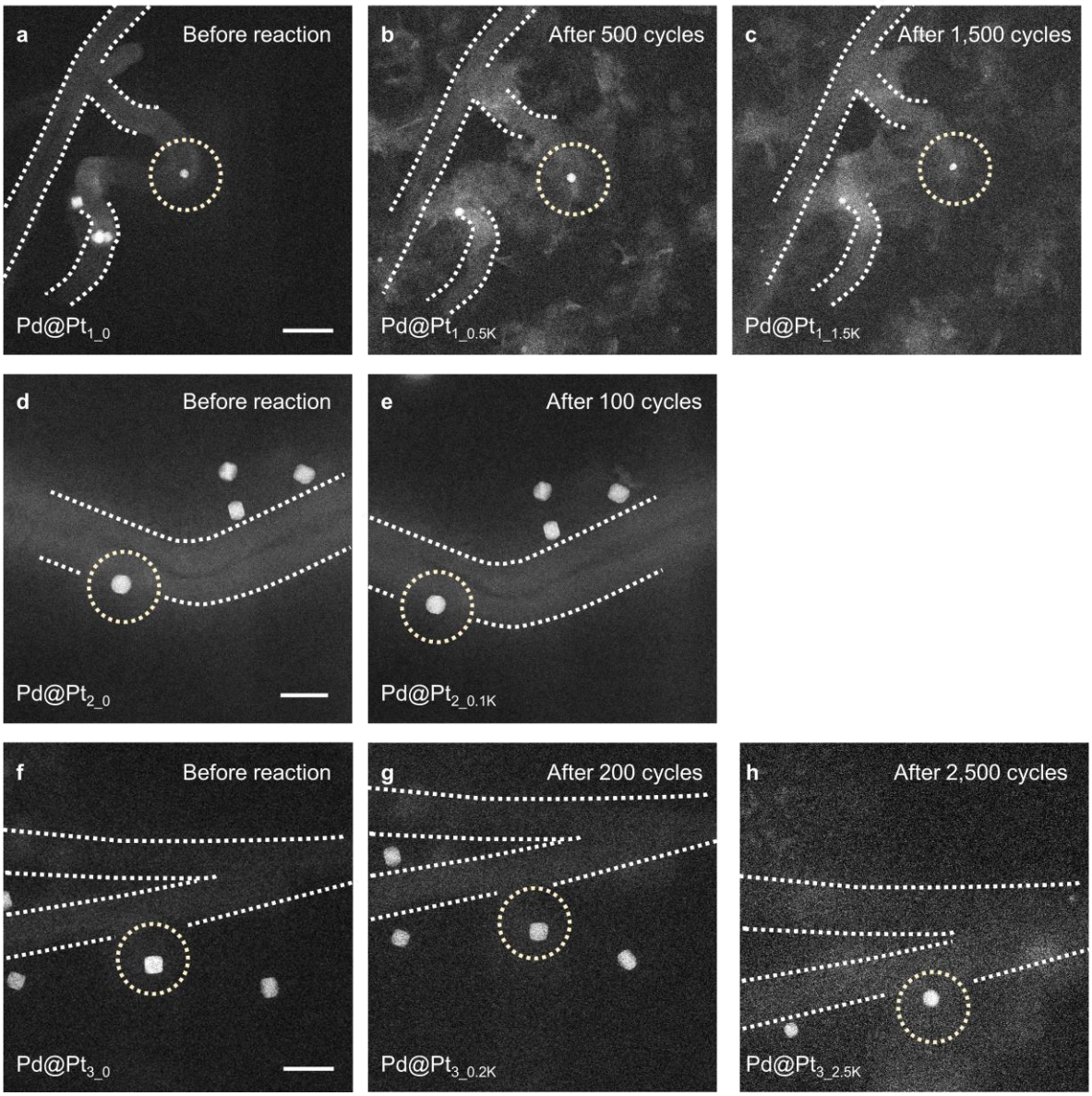

Supplementary Fig. 3 | Images around the same NPs before and after reactions. a-c, Low-magnification overview ADF-STEM images of Particle-1 recorded before reaction **(a)**, after 500 cycles **(b)** and after 1500 cycles **(c)**. Scale bars are 50 nm for **(a-c)**. **d, e,** Low-magnification overview ADF-STEM images of Particle-2 recorded before reaction (d) and after 100 cycles **(e)**. **f-h,** Low-magnification overview ADF-STEM images of Particle-3 recorded before reaction **(f)**, after 200 cycles **(g)** and after 2500 cycles **(h)**. Targeted NPs are in the center of yellow dashed circles. The intensities lighter than NPs show the shapes of surrounding carbon nanotubes (highlighted by white dashed curves), which remained intact after different cycles. Scale bars are 20 nm for **(d-h)**.

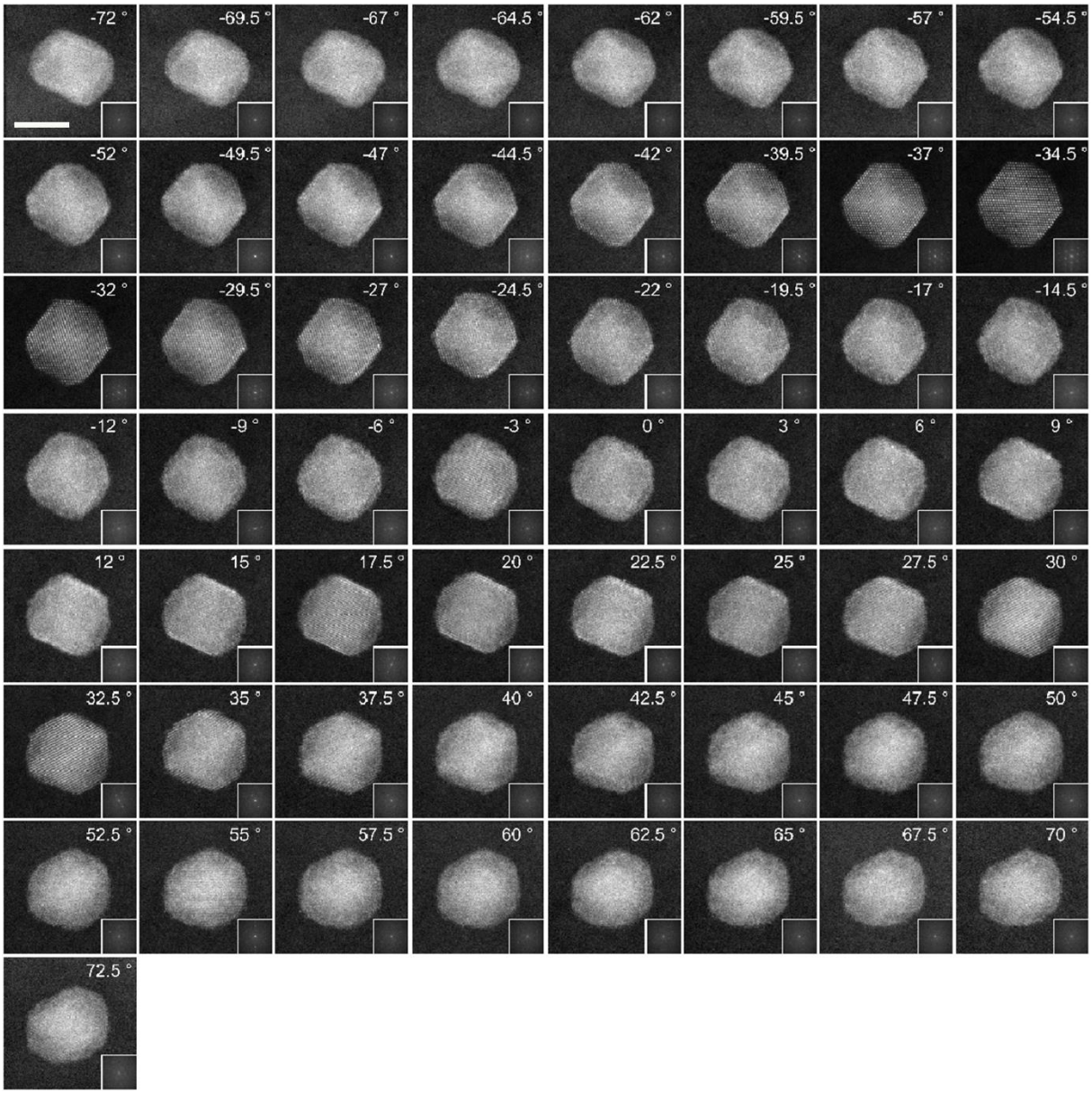

Supplementary Fig. 4 | Tomographic tilt series of Pd@Pt$_{1_0}$ NP. ADF-STEM images with a tilting range from −72.0° to +72.5°. The value of angle to which the image belongs is recorded in the upper right corner of each image. Corresponding patterns of fast fourier transform (FFT) are shown in the insets. Scale bar is 5 nm.

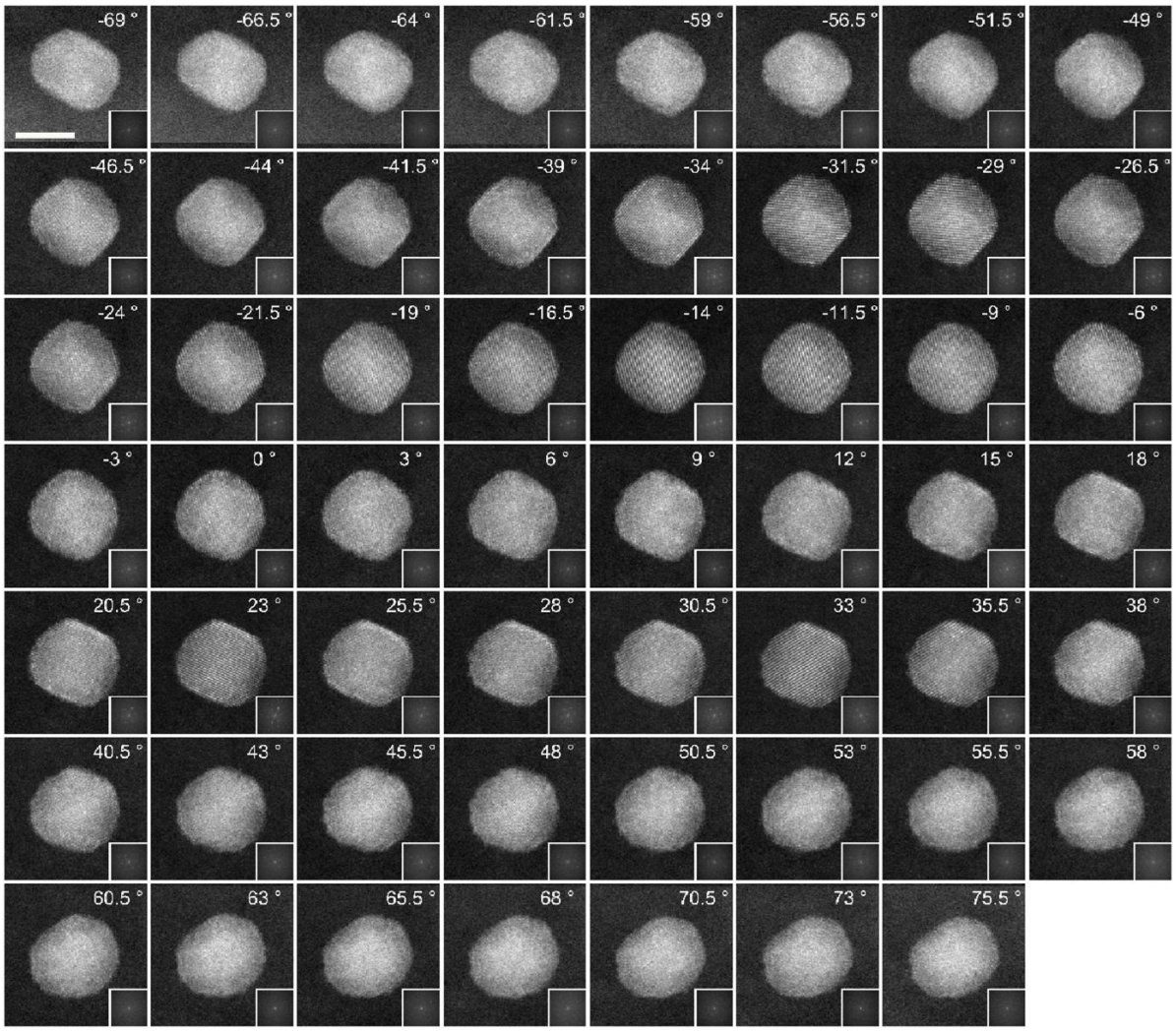

Supplementary Fig. 5 | Tomographic tilt series of Pd@Pt$_{1_0.5K}$ NP. ADF-STEM images with a tilting range from −69.0° to +75.5°. The value of angle to which the image belongs is recorded in the upper right corner of each image. Corresponding FFT patterns are shown in the insets. Scale bar is 5 nm.

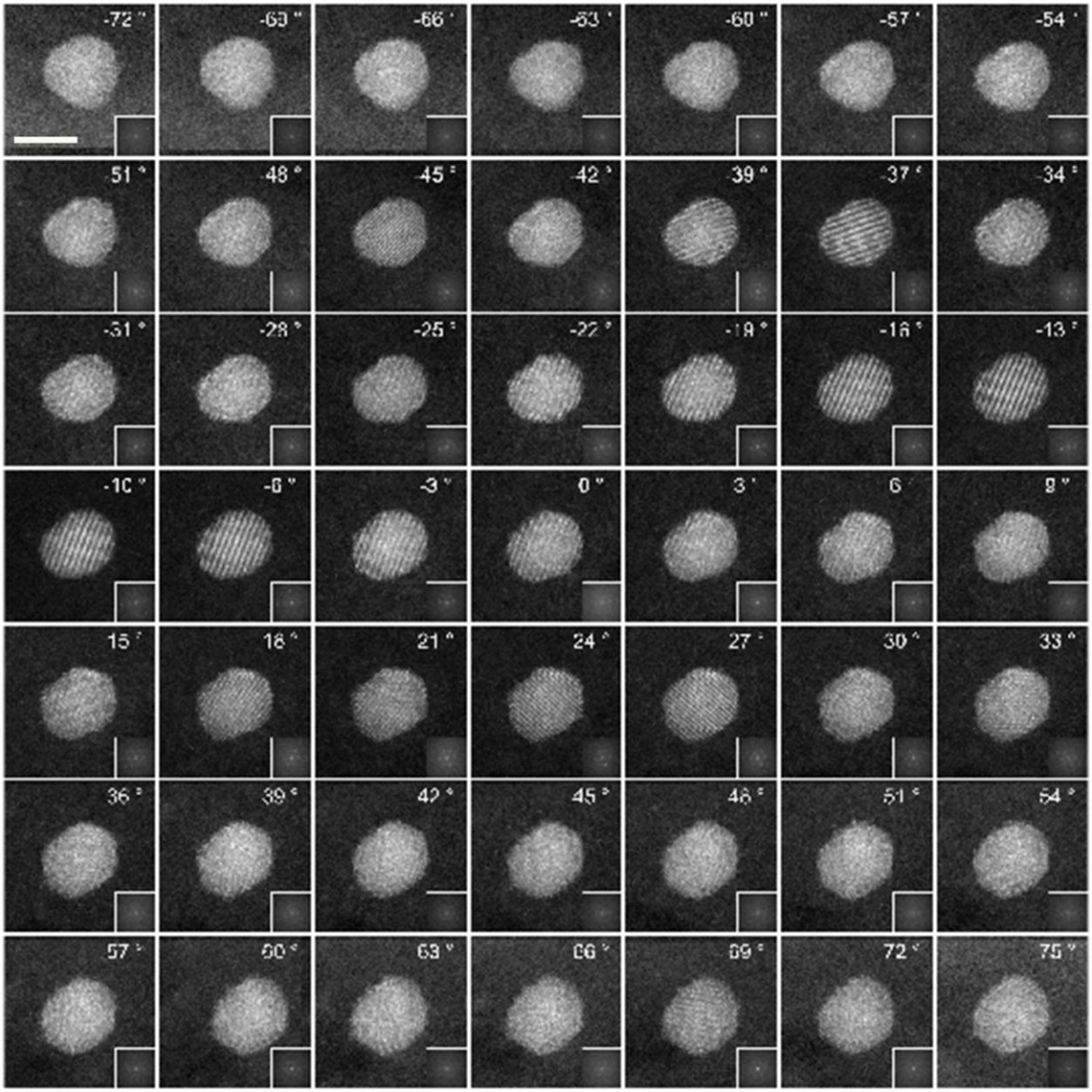

Supplementary Fig. 6 | Tomographic tilt series of Pd@Pt$_{1_1.5K}$ NP. ADF-STEM images with a tilting range from −72.0° to +75.0°. The value of angle to which the image belongs is recorded in the upper right corner of each image. Corresponding FFT patterns are shown in the insets. Scale bar is 5 nm.

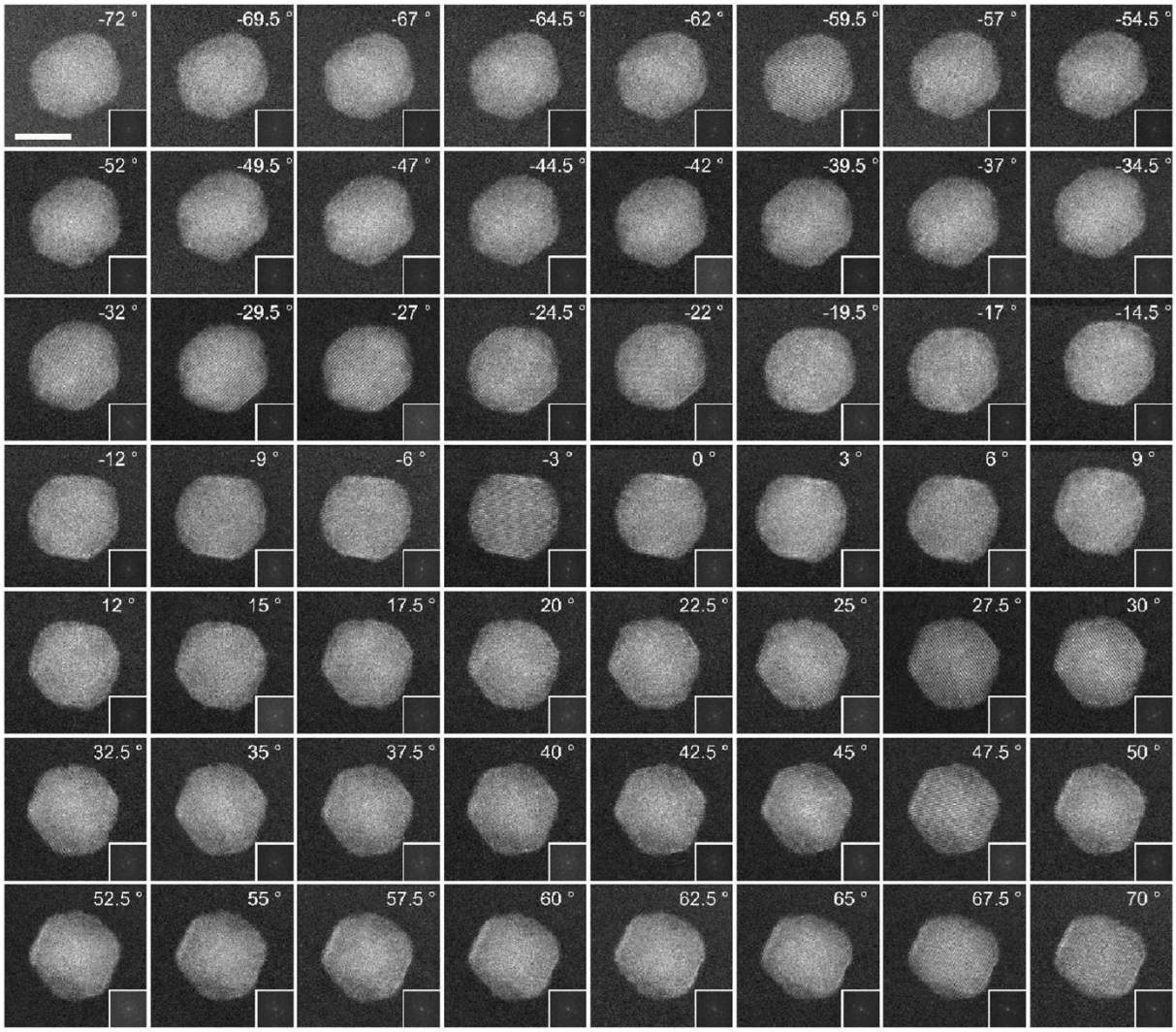

Supplementary Fig. 7 | Tomographic tilt series of Pd@Pt_{2_0} NP. ADF-STEM images with a tilting range from −72.0° to +70°. The value of angle to which the image belongs is recorded in the upper right corner of each image. Corresponding FFT patterns are shown in the insets. Scale bar is 5 nm.

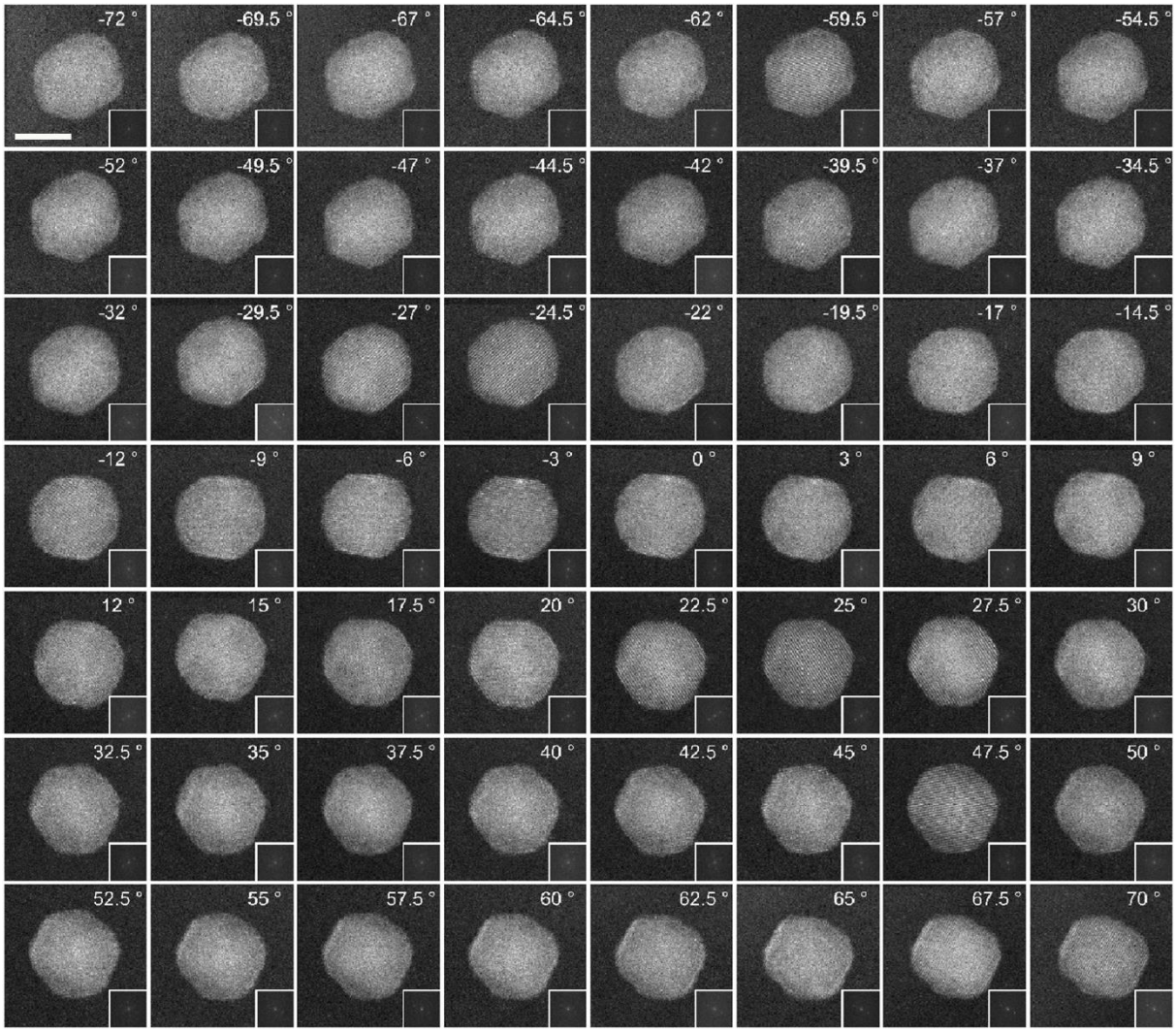

Supplementary Fig. 8 | Tomographic tilt series of Pd@Pt$_{2_0.1K}$ NP. ADF-STEM images with a tilting range from −72.0°to +70.0°. The value of angle to which the image belongs is recorded in the upper right corner of each image. Corresponding FFT patterns are shown in the insets. Scale bar is 5 nm.

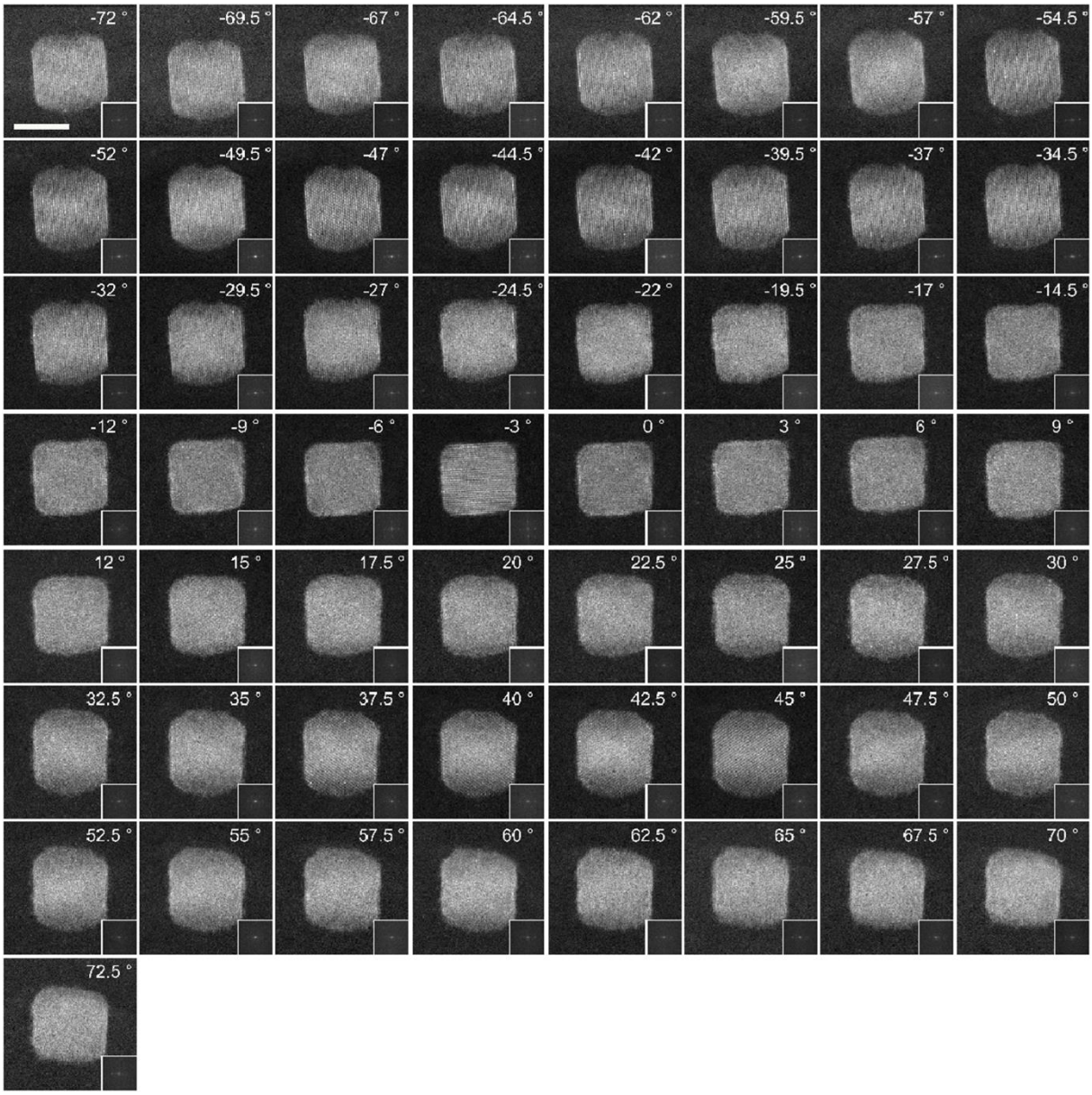

Supplementary Fig. 9 | Tomographic tilt series of Pd@Pt_{3_0} NP. ADF-STEM images with a tilting range from −72.0°to +72.5°. The value of angle to which the image belongs is recorded in the upper right corner of each image. Corresponding FFT patterns are shown in the insets. Scale bar is 5 nm.

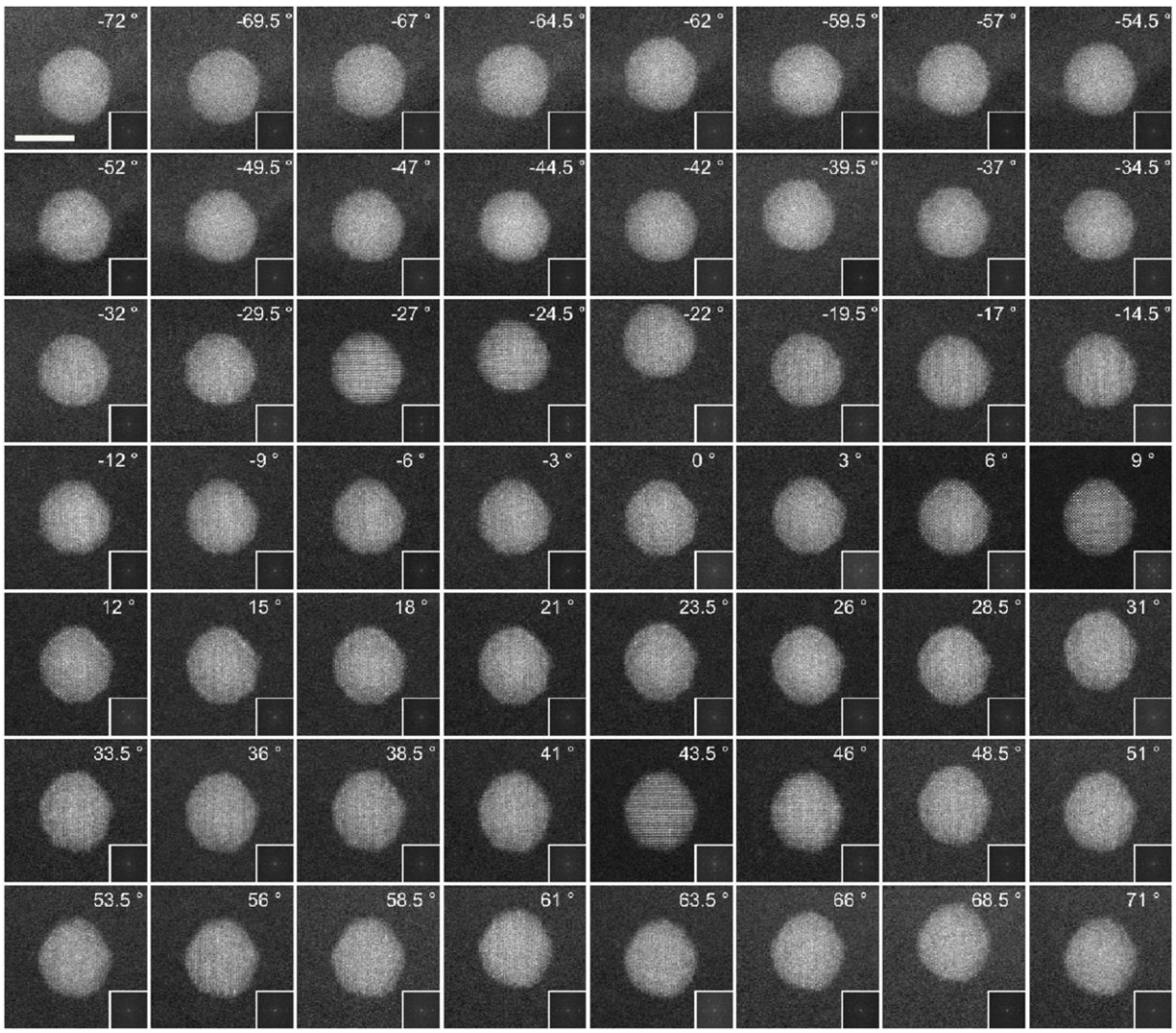

Supplementary Fig. 10 | Tomographic tilt series of Pd@$Pt_{3\_2.5K}$ NP. ADF-STEM images with a tilting range from −72.0°to +71.0°. The value of angle to which the image belongs is recorded in the upper right corner of each image. Corresponding FFT patterns are shown in the insets. Scale bar is 5 nm.

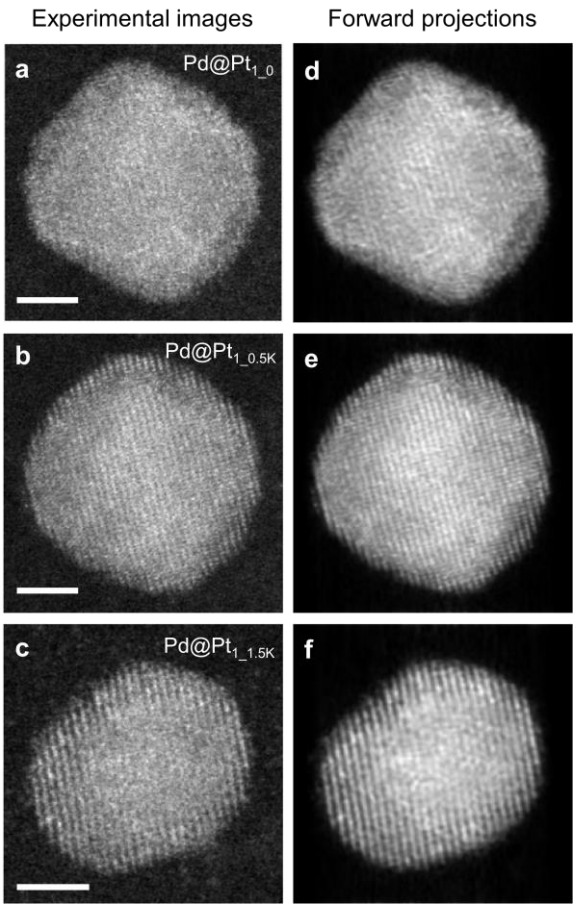

Supplementary Fig. 11 | Consistency check of Particle-1 series. a-c, ADF-STEM images taken at 0° during tilting experiment for Pd@Pt_{1_0} **(a)**, Pd@$Pt_{1\_0.5K}$ **(b)** and Pd@$Pt_{1\_1.5K}$ **(c)**, respectively. **d-f,** Simulated forward projections of the final 3D atomic model at the tilt angles for Pd@Pt_{1_0} **(d)**, Pd@$Pt_{1\_0.5K}$ **(e)** and Pd@$Pt_{1\_1.5K}$ **(f)**, respectively. Scale bars are 2 nm.

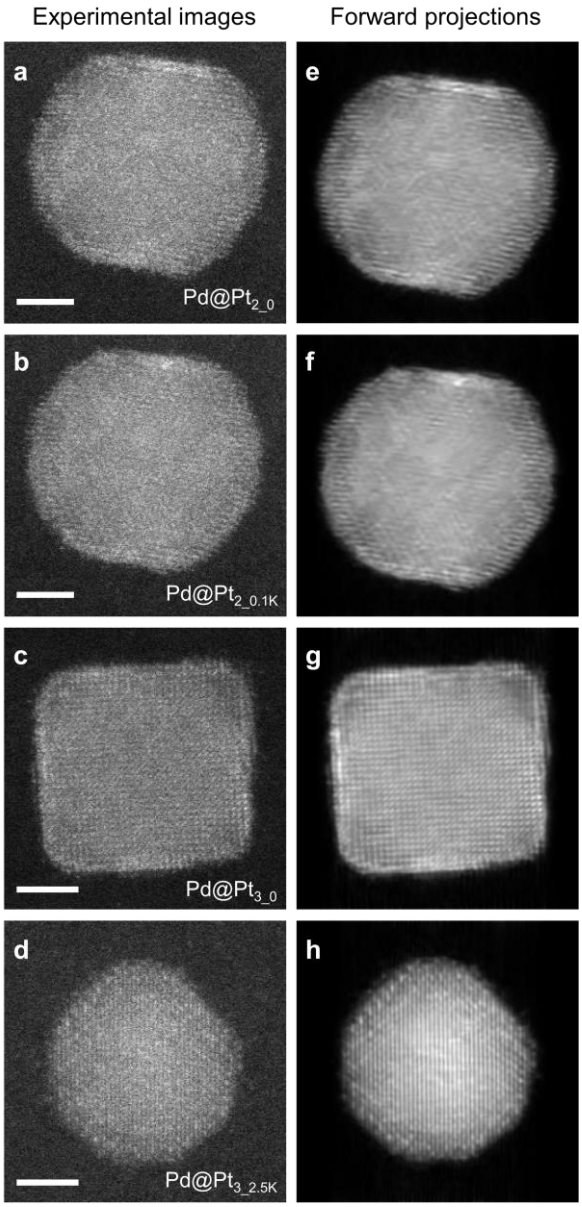

Supplementary Fig. 12 | Consistency check of Particle-2 and -3 series. a-c, ADF-STEM images taken at 0° during tilting experiment for Pd@Pt_{2_0} **(a)**, Pd@$Pt_{2\_0.1K}$ **(b)**, Pd@Pt_{3_0} **(c)** and Pd@$Pt_{3\_2.5K}$ **(d)**, respectively. **e-h,** Simulated forward projections of the final 3D atomic model at the tilt angles for Pd@Pt_{2_0} **(e)**, Pd@$Pt_{2\_0.1K}$ **(f)**, Pd@Pt_{3_0} **(g)** and Pd@$Pt_{3\_2.5K}$ **(h)**, respectively. Scale bars are 2 nm.

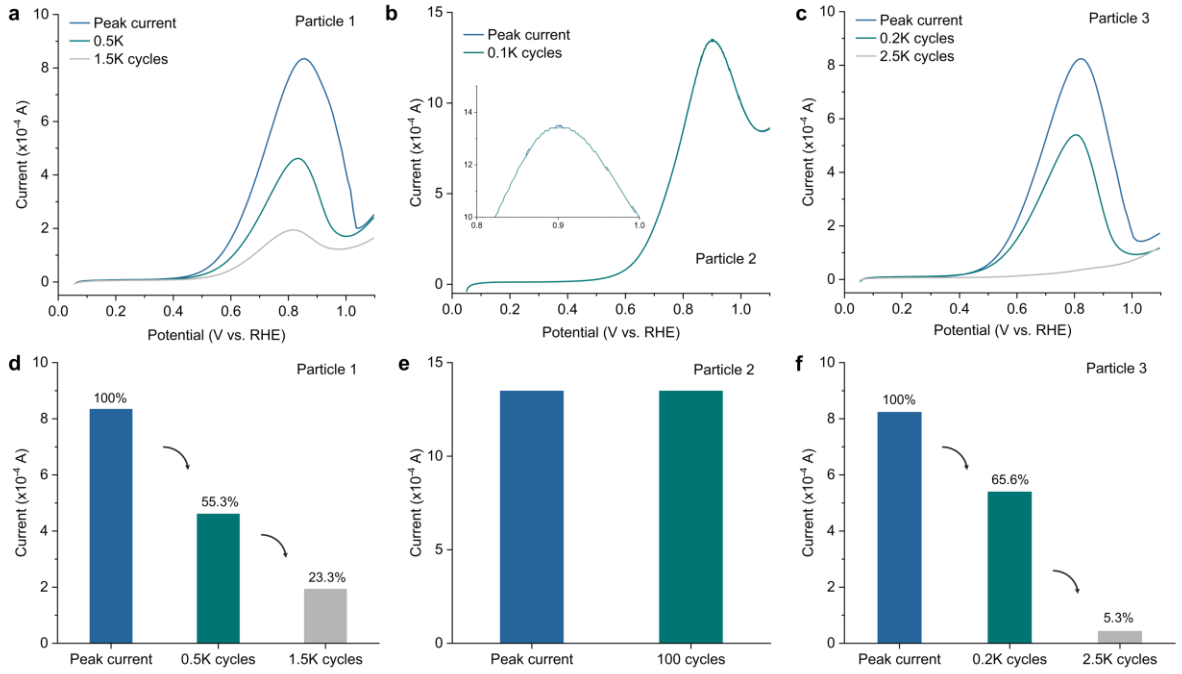

Supplementary Fig. 13 | Electrocatalytic results for Pd@Pt/CNT nanocatalysts at different periods of ethanol oxidation reaction.

a-c, CV curves of Particle-1 **(a)**, Particle-2 **(b)** and Particle-3 **(c)**. **d-f,** Current values of Particle-1 **(d)**, Particle-2 **(e)** and Particle-3 **(f)**. For Particle-1, the current decayed from 0.84 mA (peak current, after 122 cycles) to 0.46 mA (after 500 cycles) and to 0.20 mA (after 1500 cycles). Particle-2 is recorded right after the activation, the current after 100 cycles is equal to the peak current (1.35 mA). Peak current in Particle-2 occurs after 99 cycles. For Particle-3, the current decayed from 0.82 mA (peak current, after 103 cycles) to 0.54 mA (after 200 cycles) and to 0.04 mA (after 2500 cycles). The peak currents are similar between experimental batches of Particle-1 and Particle-3, with the same amount of catalyst inks on the grid. Under identical catalyst loadings, the peak currents for Particle-1 and Particle-3 are similar, demonstrating good reproducibility across experimental batches. Due to a higher catalyst loading on the grid, Particle-2 exhibited a greater peak current than both Particle-1 and Particle-3 (Supplementary Table 1).

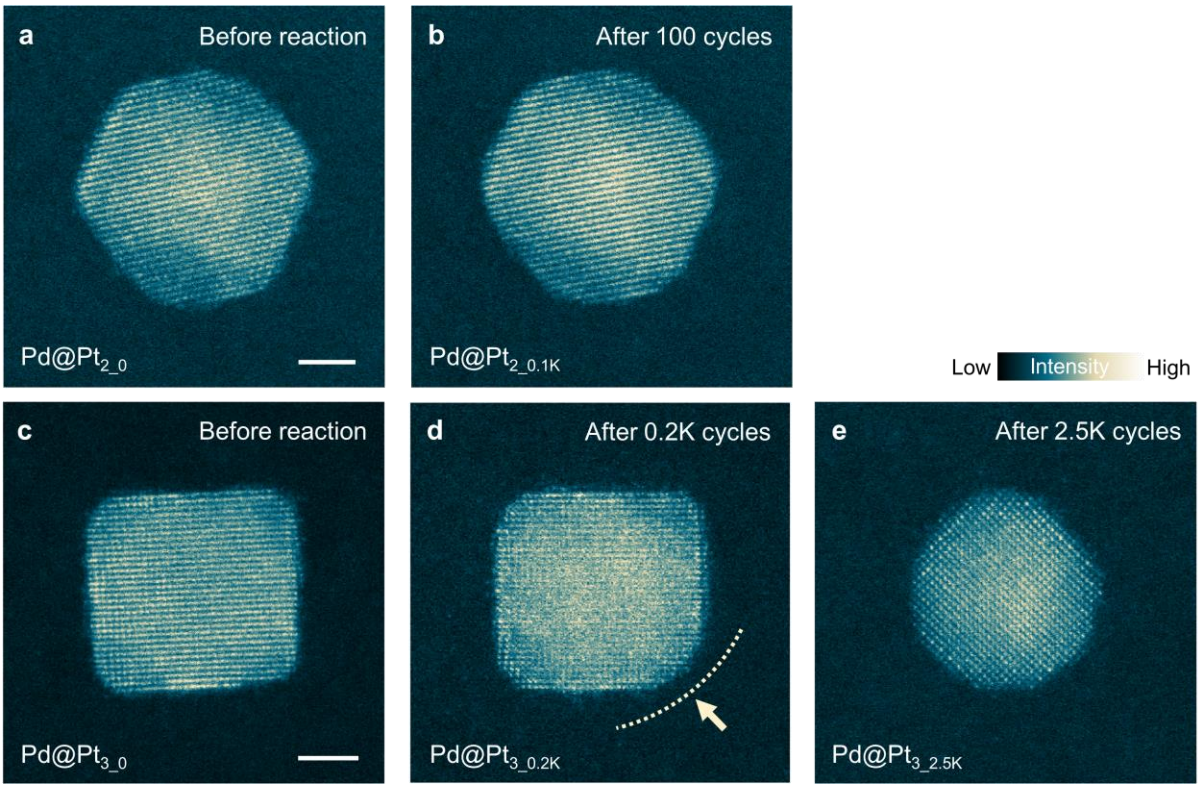

Supplementary Fig. 14 | Representative images of Particles 2 & 3 with similar zone axis at different cycles. a, b, ADF-STEM images from tomographic tilt-series of Particle-2 before reaction **(a)** and after 100 cycles **(b)**. The tilting angles for both of the images are 47.5°. **c-e,** ADF-STEM images from tomographic tilt-series of Particle-3 before reaction **(c)**, after 200 cycles **(d)** and after 2500 cycles **(e)**. The tilting angles for the images are -3° **(c)**, 6° **(d)** and -9° **(e)**, respectively. Images were registered and averaged from three sequential frames at the same tilting angles. The colormap represents intensities of the raw images. Scale bars are 2 nm. Since Particle-3 at 200 cycles had already attained a rounded morphology—indicating a similar reconstruction stage as seen in Pd@$Pt_{1\_0.5K}$ and Pd@$Pt_{2\_0.1K}$—we proceeded directly to 2.5K cycles to probe the deeper degradation regime and its 3D structural evolution.

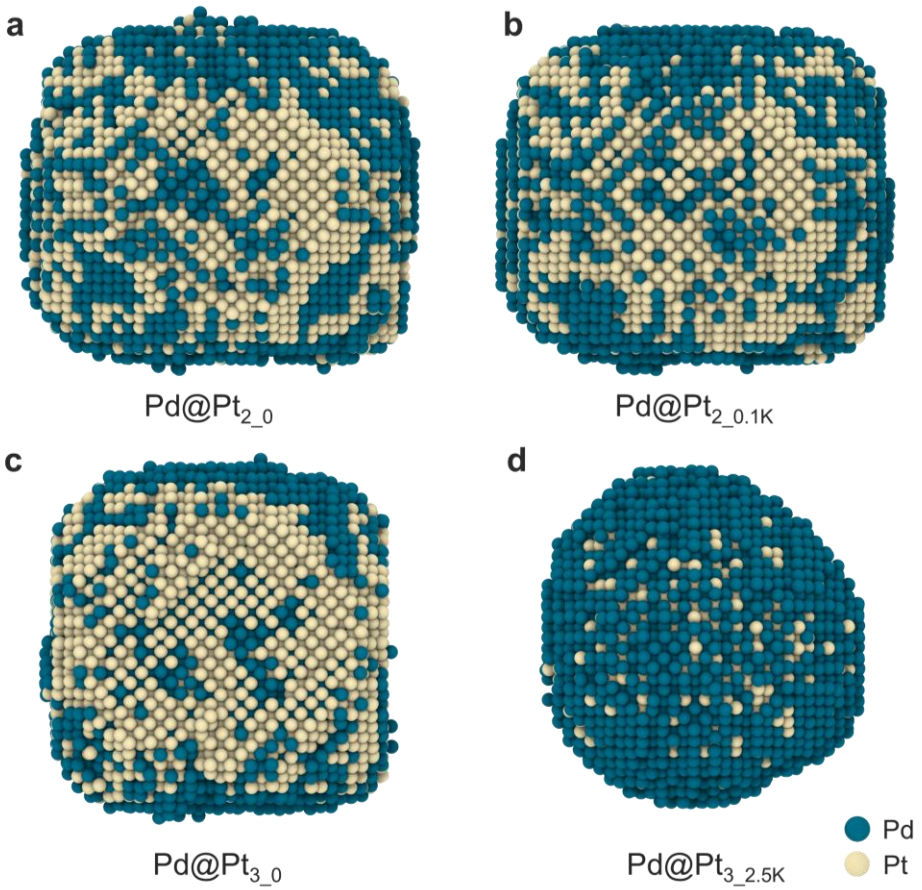

Supplementary Fig. 15 | The 3D atomic models of Particles 2 & 3. a, b, Experimental 3D atomic models of Particle-2: Pd@Pt_{2_0} **(a)** and Pd@$Pt_{2\_0.1K}$ **(b)**. A certain degree of surface reconstruction was observed at the near-surface region. **c, d,** Experimental 3D atomic models of Particle-3: Pd@Pt_{3_0} **(c)** and Pd@$Pt_{3\_2.5K}$ **(d)**. Green and yellow spheres represent Pd and Pt atoms, respectively. A drastic structural transformation occurs after 2.5K cycles, characterized by severe atom leaching and subsequent Pd segregation.

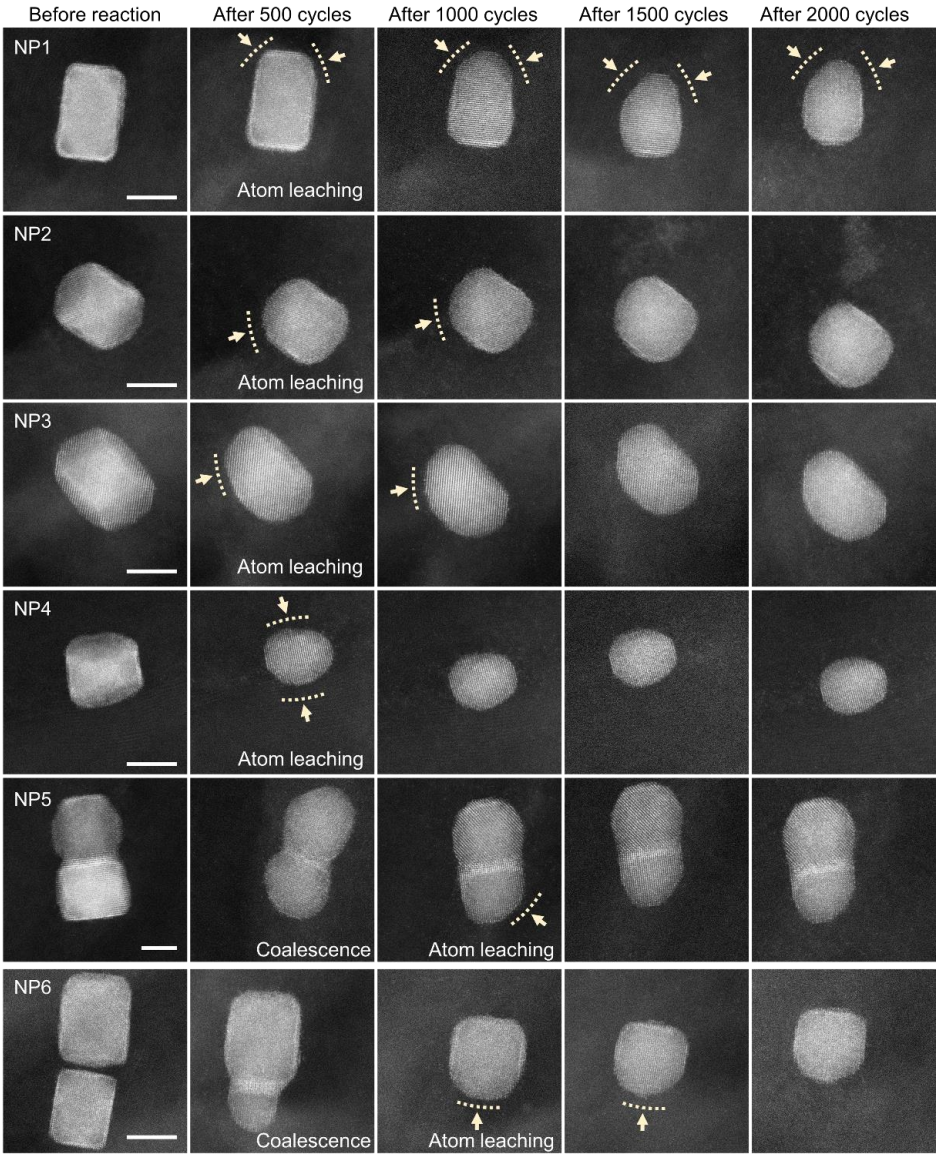

Supplementary Fig. 16 | Ex situ observations of six batches of NPs before and after 500-2000 cycles. Scale bars are 5 nm. From up to bottom, each row represents one batch of NP, named as NP1, 2, 3, 4, 5 and 6, respectively. From left to right, each of the NP was imaged before reaction and after 500, 1000, 1500 and 2000 cycles, respectively. For NP1-4, obvious structural changes were observed at continuous cycles. For NP5 and NP6, coalescences of two adjacent NPs were observed after 500 cycles. Subsequently, from 1000 to 2000 cycles, the coalesced structures underwent further degradation dominated by atom leaching, consistent with the primary pathway identified in other particles.

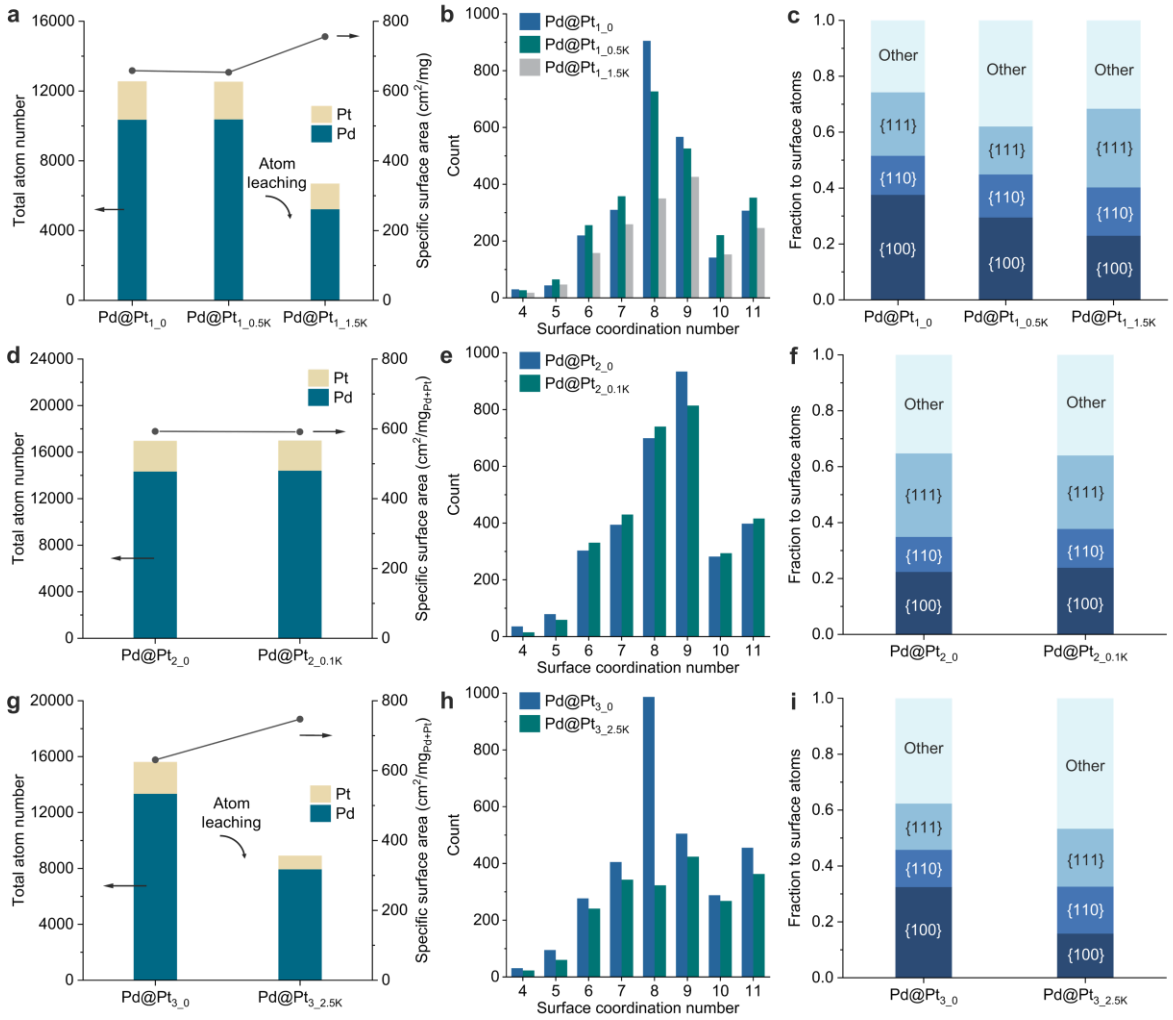

Supplementary Fig. 17 | Basic structural analysis of Pd@Pt Particle 1-3 series. a-c, Information of total atom numbers **(a)** and specific surface areas, surface coordination number **(b)** and surface facet distribution **(c)** of Particle-1. **d-f,** Information of total atom numbers and specific surface areas **(d)**, surface coordination number **(e)** and surface facet distribution **(f)** of Particle-2. **g-i,** Information of total atom numbers and specific surface areas **(g)**, surface coordination number **(h)** and surface facet distribution **(i)** of Particle-3.

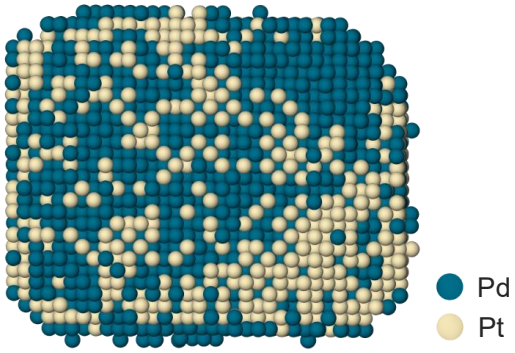

Supplementary Fig. 18 | Chemical consistent core between Pd@Pt$_{1_0}$ and Pd@Pt$_{1_0.5K}$. Green and yellow represent Pd and Pt, respectively.

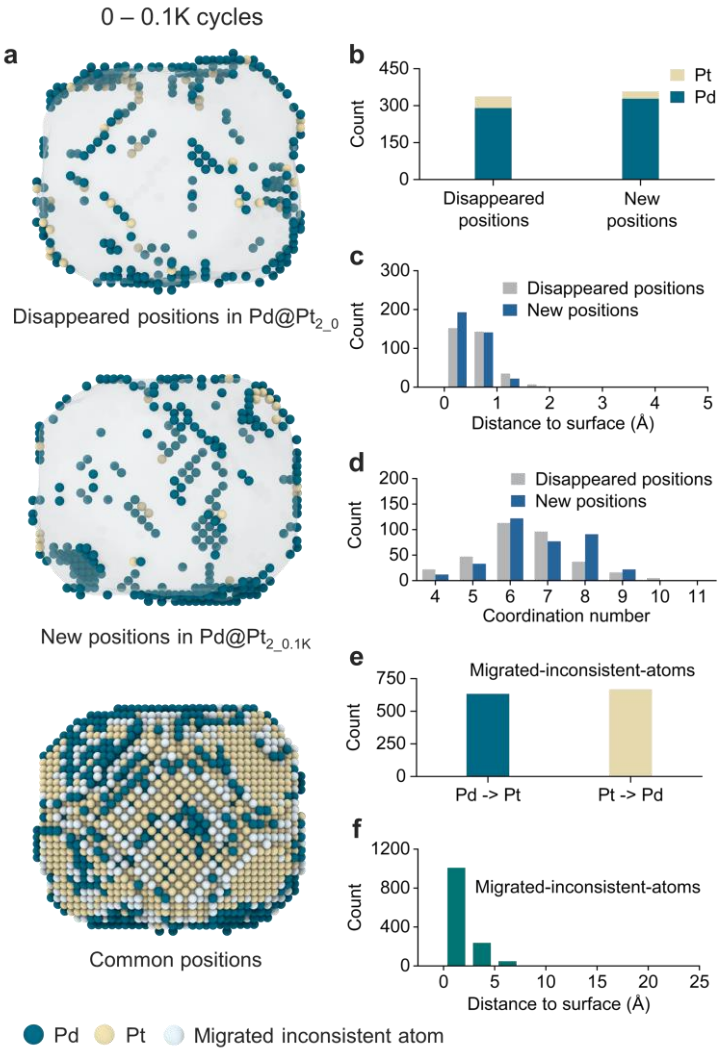

Supplementary Fig. 19 | 4D evolution of atomic positions and chemical species in Particle-2. a, 3D renderings of Particle-2 at surface reconstruction before and after 100 cycles. Upper panel shows the atoms that are identified in Pd@Pt$_{2_0}$ but absent in later stages, named as disappeared positions; central panel shows the atoms newly identified in Pd@Pt$_{2_0.1K}$, named as new positions; lower panel show the conserved atoms that are present in both in Pd@Pt$_{2_0}$ and Pd@Pt$_{2_0.1K}$, named as common positions. **b-d,** Statistic structural analysis of unpaired atoms before and after 100 cycles: total numbers **(b)**, distribution of distances to surface **(c)**, and distribution of coordination number of disappeared and new positions **(d)**. **e, f,** Migrated-inconsistent-atoms at common positions before and after 100 cycles. Total numbers **(e)** and distribution of distances to surface **(f)**. Green, yellow, and white spheres represent Pd, Pt, and migrated-inconsistent-atoms at the common positions, respectively.

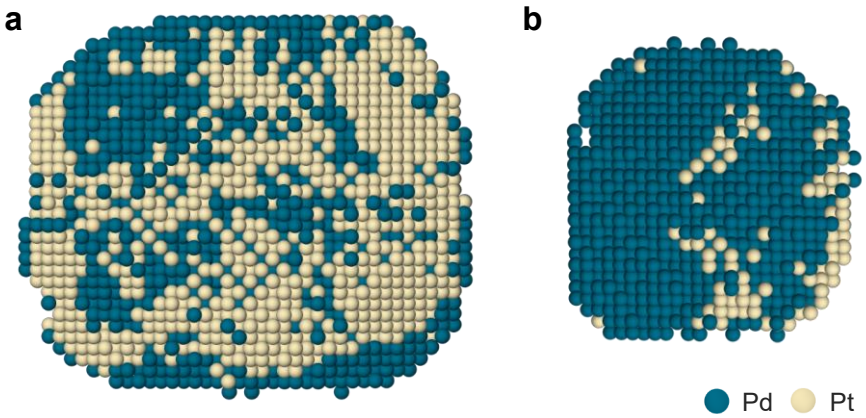

Supplementary Fig. 20 | Chemical consistent cores. a, Chemical consistent core between Pd@Pt_{2_0} and Pd@$Pt_{2\_0.1K}$. **b,** Chemical consistent core between Pd@$Pt_{1\_0.5K}$ and Pd@$Pt_{1\_1.5K}$. Green and yellow represent Pd and Pt, respectively.

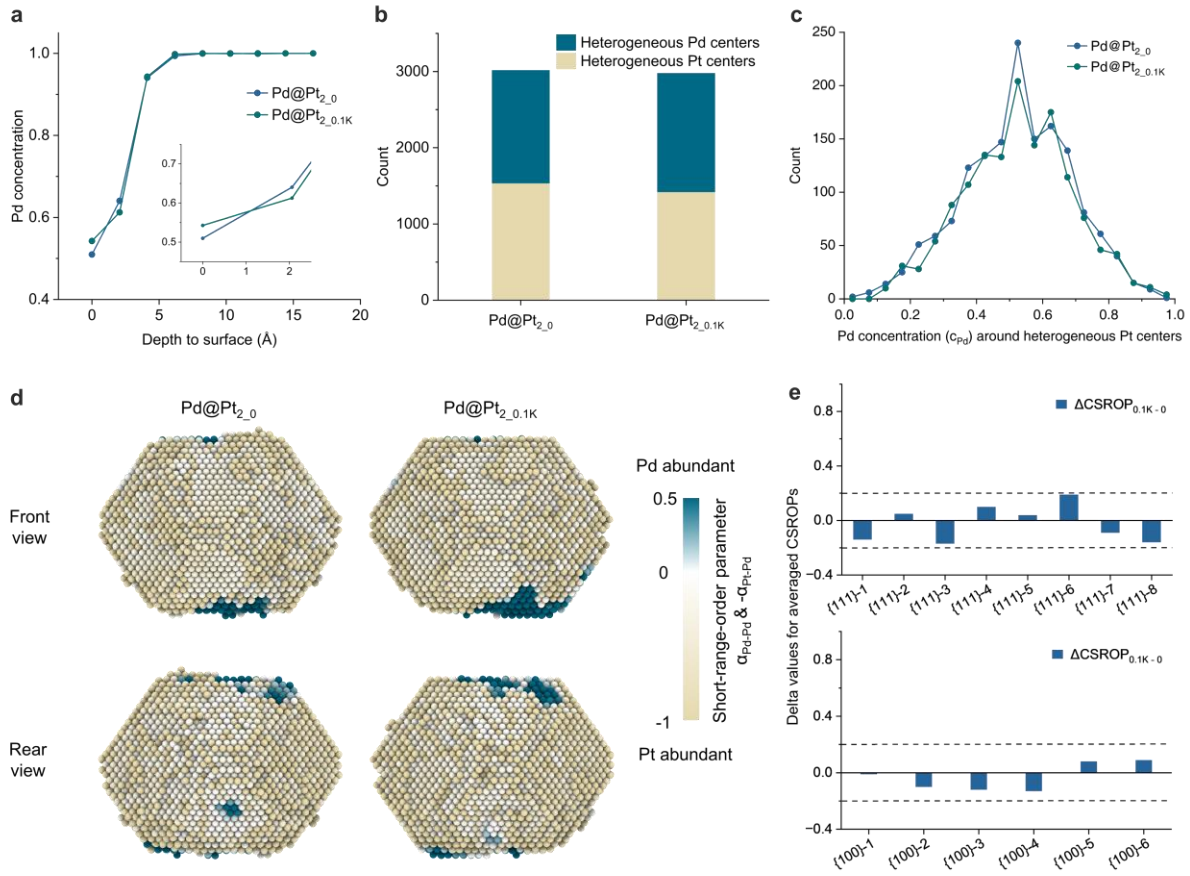

Supplementary Fig. 21 | Evolution of chemical heterogeneity and short-range-order in particle-2. a, Shell-by-shell Pd concentrations at different cycles. **b,** Number of heterogeneous centers. A heterogeneous center is defined as one atom coordinated by both Pd and Pt neighbors. **c,** Overall distribution of local Pd concentrations (c_{Pd}) around heterogeneous Pt centers. c_{Pd} (x axis) represents Pd/(Pd+Pt) atomic fractions in coordination shells, indicating local Pd occurrence probabilities around central atoms. **d,** 3D renderings of CSROP in Particle-2 viewed from the front and rear sides at different cycles. Green, yellow and white colormap represent the Pd-abundant regions, the Pt-abundant regions and the regions with the averaged Pd concentration in the whole particle, respectively. Colormap values are normalized to -1 to 0.5. **e,** Delta values for the orientation-classified averages of CSROPs (ΔCSROPs). Surface atoms were segmented into eight {111} orientations (upper panel) and six {100} orientations (lower panel). The CSROP was first averaged within each region (Supplementary Fig. 23). Then ΔCSROP was then calculated for the interval between $Pd@Pt_{2\_0.1K}$ and $Pd@Pt_{2\_0}$.

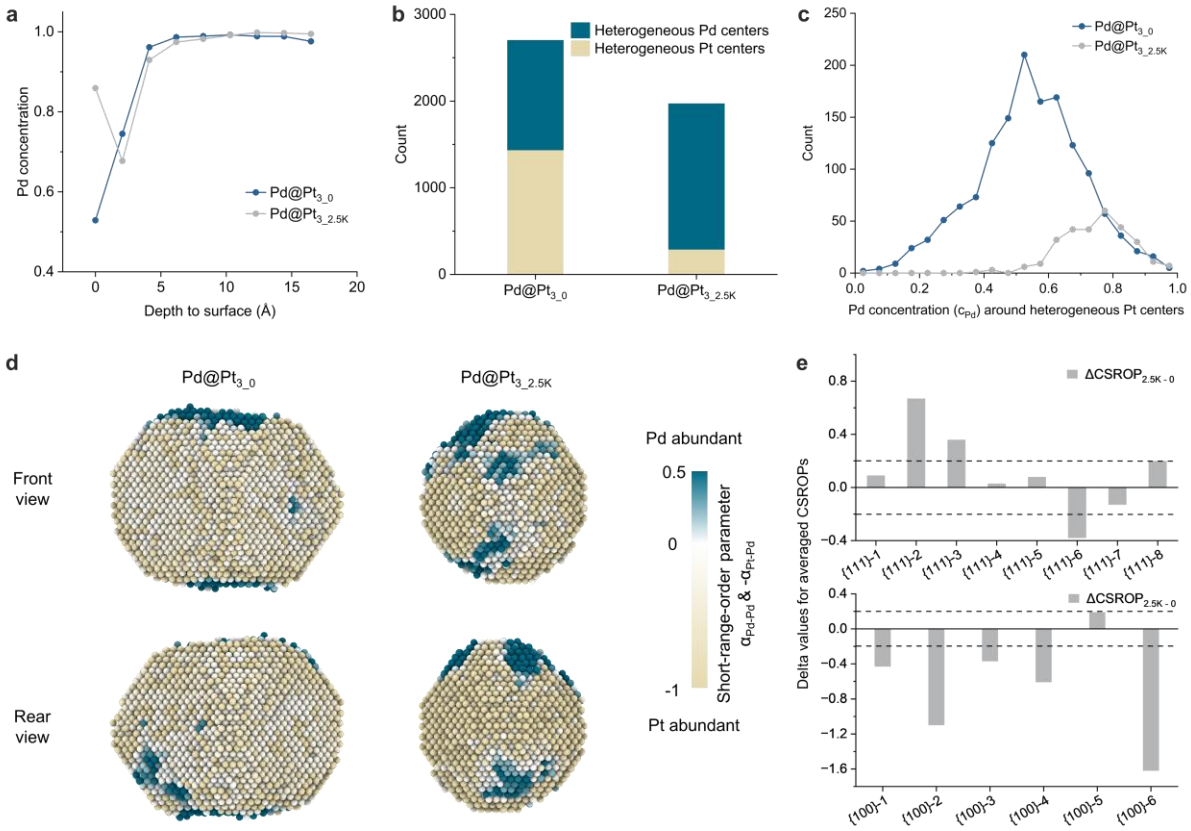

Supplementary Fig. 22 | Evolutions of chemical heterogeneity and CSROP for Particle-3. **a,** Shell-by-shell Pd concentrations at different cycles. **b,** Number of heterogeneous centers. A heterogeneous center is defined as one atom coordinated by both Pd and Pt neighbors. **c,** Overall distribution of local Pd concentrations (c_{Pd}) around heterogeneous Pt centers. c_{Pd} (x axis) represents Pd/(Pd+Pt) atomic fractions in coordination shells, indicating local Pd occurrence probabilities around central atoms. **d,** 3D renderings of CSROP in Particle-3 viewed from the front and rear sides at different cycles. Green, yellow and white colormap represent the Pd-abundant regions, the Pt-abundant regions and the regions with the averaged Pd concentration in the whole particle, respectively. Colormap values are normalized to -1 to 0.5. **e,** Delta values for the orientation-classified averages of CSROPs (ΔCSROPs). Surface atoms were segmented into eight {111} orientations (upper panel) and six {100} orientations (lower panel). The CSROP was first averaged within each region (Supplementary Fig. 23). Then ΔCSROP was then calculated for the interval between $Pd@Pt_{3\_2.5K}$ and $Pd@Pt_{3\_0}$.

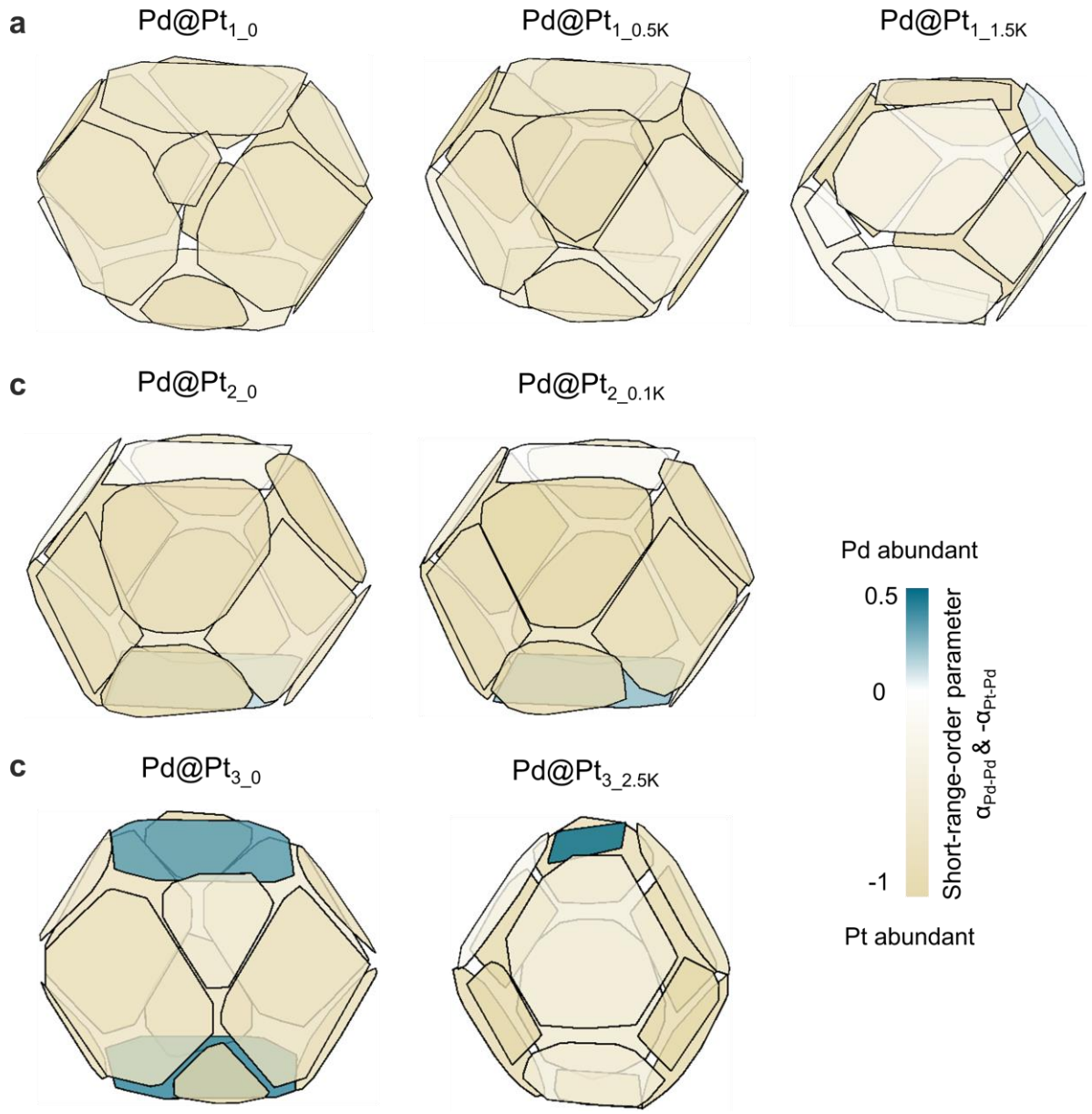

Supplementary Fig. 23 | Renderings of CSROPs in different orientations. a-c, CSROPs of Particle-1 **(a)**, Particle-2 **(b)** and Particle-3 **(c)**, respectively. Green, yellow and white colormaps represent the Pd-abundant regions, the Pt-abundant regions and the regions with the averaged Pd concentration in the whole particle, respectively. Colormap values are normalized to -1 to 0.5.

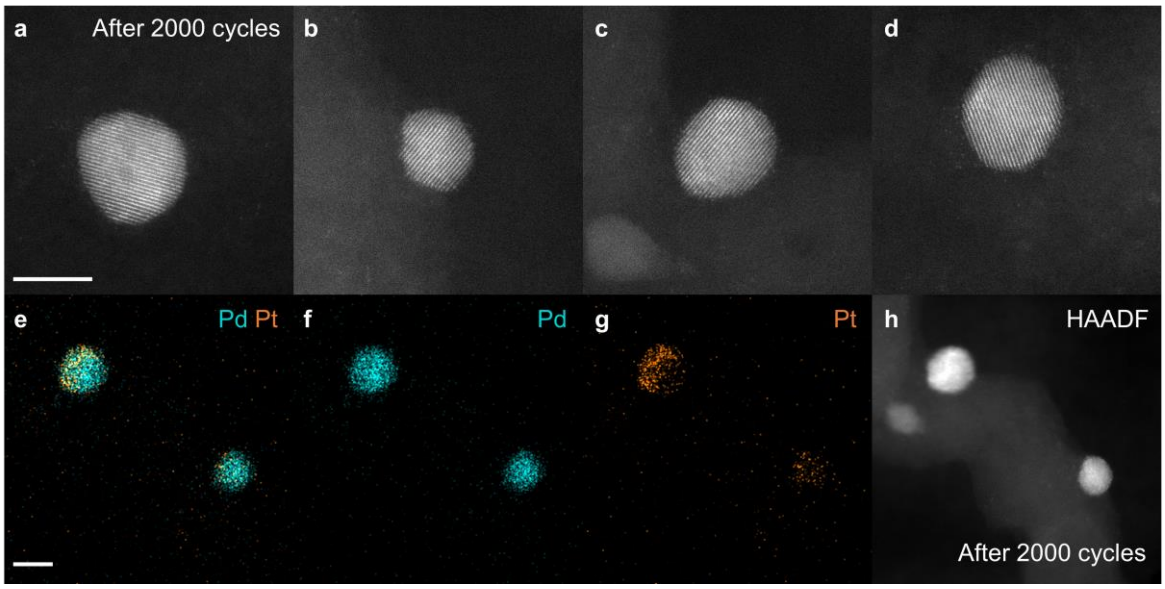

Supplementary Fig. 24 | Characterization of Pd@Pt/CNT nanocatalysts after 2000 cycles. **a-d,** ADF-STEM images of Pd@Pt after 2000 cycles. **e-h,** EDS mapping of Pd@Pt/CNT nanocatalysts after 2000 cycles: images of merged Pd and Pt signals **(e)**, Pd **(f)**, Pt **(g)** and ADF **(h)** signals. Scale bars are 5 nm. The core-shell features are lost and the sizes of NPs are smaller after long cycles. Pt signals of NP in **(e)** and **(g)** show asymmetric distribution, which indicates the exist of element redistribution after long cycles.

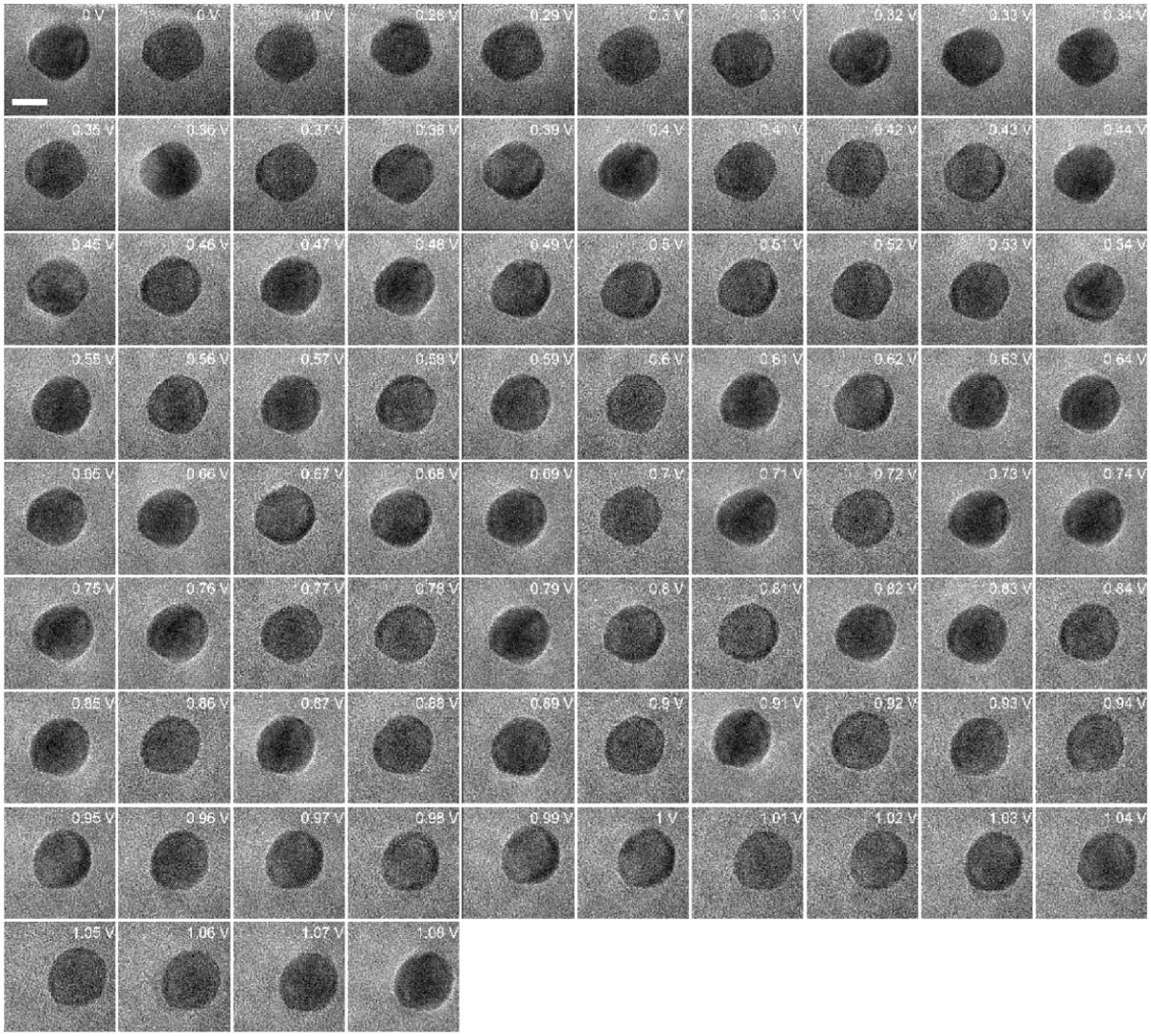

Supplementary Fig. 25 | Voltage-sequential in situ TEM images of morphological evolution under CV condition. TEM images before and during CV conditions from 0.28 V_{RHE} to 1.08 V_{RHE}. Scale bar for all panels is 5 nm.

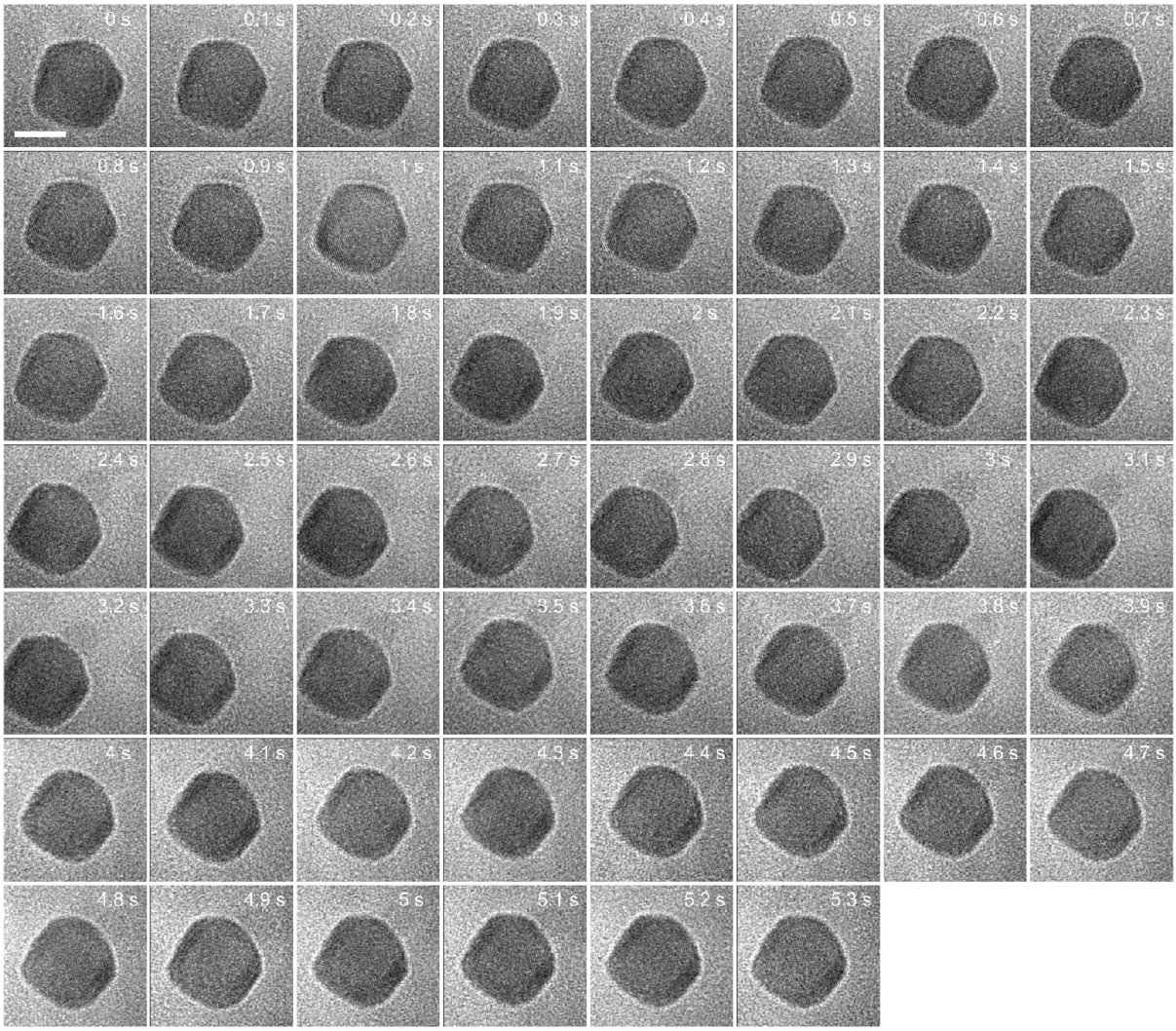

Supplementary Fig. 26 | Time-sequential in situ TEM images of morphological evolution under chronoamperometry (CA) condition at 0.68 V_{RHE}. We kept the interested region (upper right region of the NP) always in the field of view, while part of the NP drifted out of the field of view. Scale bar for all panels is 5 nm.

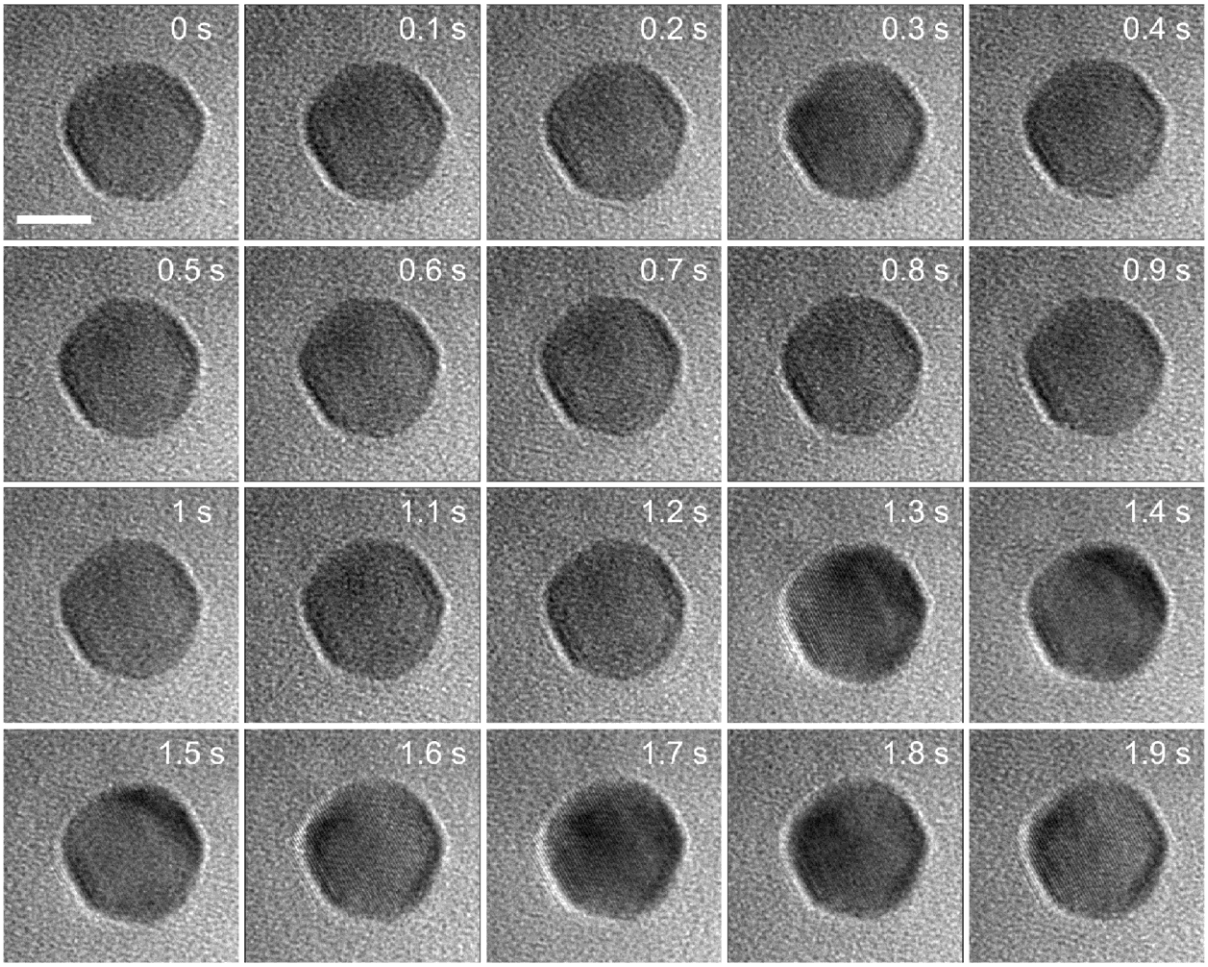

Supplementary Fig. 27 | Time-sequential in situ TEM images of morphological evolution under CA condition at 0.68 V_{RHE}. Scale bar for all panels is 5 nm.

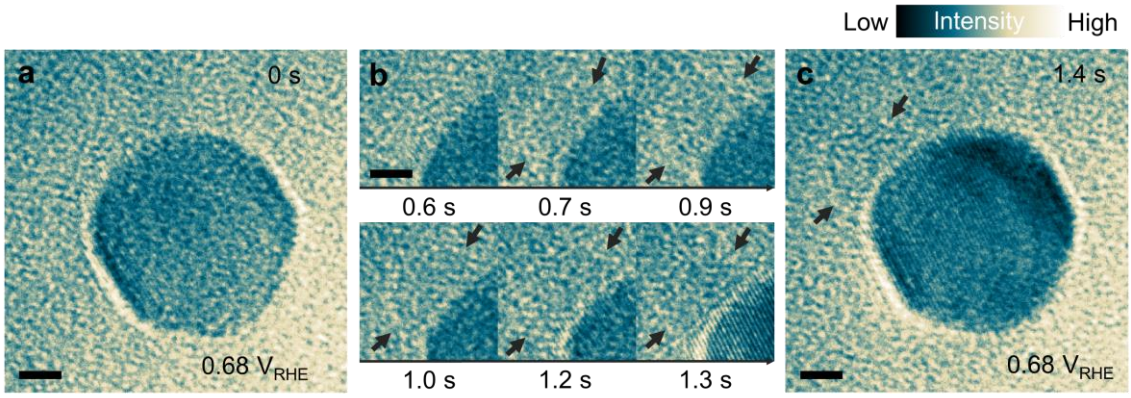

Supplementary Fig. 28 | Time-sequential in situ TEM images under a voltage of 0.68 V_{RHE}. TEM images before **(a)** and during **(b, c)** atom leaching happens. Arrows point to the locations of fluctuating clusters. Colormap is placed above **(c)**. Scale bars are 2 nm.

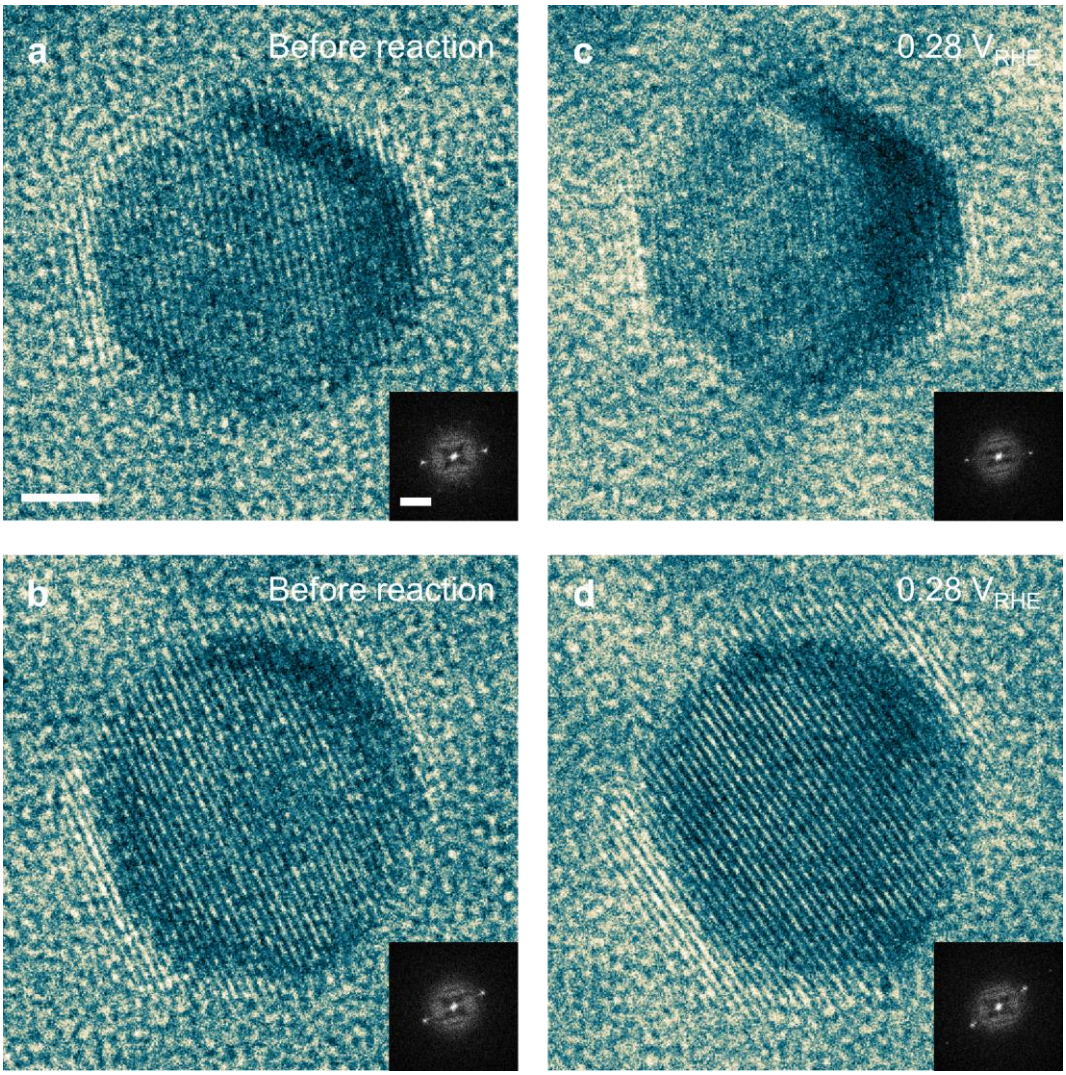

Supplementary Fig. 29 | In situ electrochemical TEM observations for two NPs before and under CA test with a lower potential of 0.28 V_{RHE}. a-d, TEM images before **(a, b)** and during **(c, d)** CA test. Corresponding FFT patterns are shown in the insets. Scale bar for all panels is 2 nm.

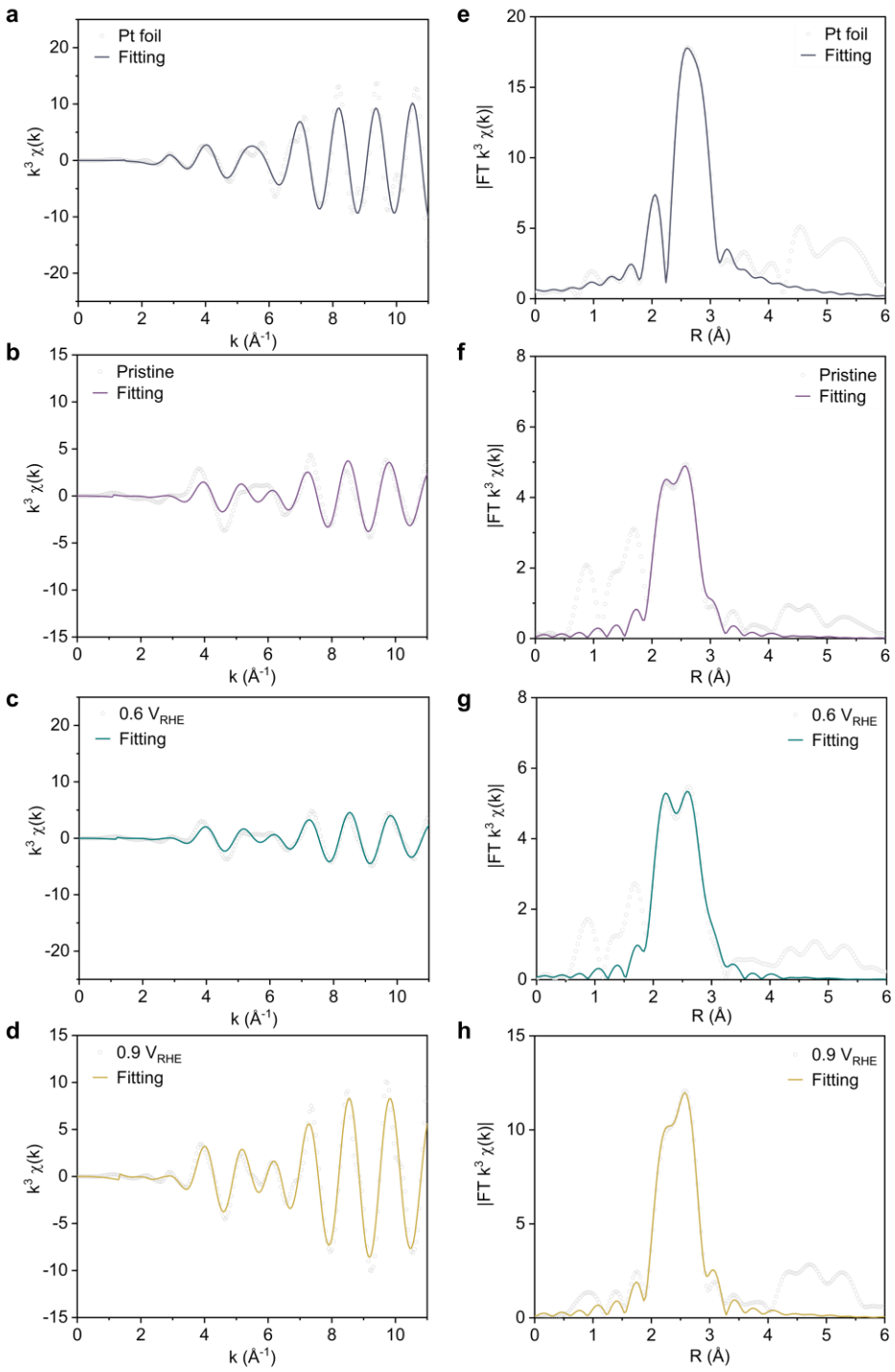

Supplementary Fig. 30 | a-h, The *k* space **(a-d)** and *R* space **(e-h)** fitting results of Pt L_3-edge for Pt foil **(a, e)**, Pd@Pt before EOR test **(b, f)**, Pd@Pt after CA test at 0.6 V_{RHE} for 6 h **(c, g)** and Pd@Pt after CA test at 0.9 V_{RHE} for 2 h **(d, h)**, respectively.

Supplementary Movie 1
Raw TEM images in Fig. 4a-c and Supplementary Fig. 25, under CV condition from 0.28 V_{RHE} to 1.08 V_{RHE}. The arrow in the movie points to the rounded places.

Supplementary Movie 2.
Raw TEM images in Fig. 4f-h and Supplementary Fig. 26, under CA condition at 0.68 V_{RHE}. The arrow in the movie points to the locations of fluctuating clusters.

Supplementary Movie 3.
Raw TEM images in Supplementary Figs. 27-28, under CA condition at 0.68 V_{RHE}. The arrow in the movie points to the locations of fluctuating clusters.

Supplementary Movie 4.
Raw TEM images in Supplementary Fig. 29a-b, with no bias.

Supplementary Movie 5.
Raw TEM images in Supplementary Fig. 29c-d, under CA condition at 0.28 V_{RHE}.

Reference

1. Pham, M., Yuan, Y., Rana, A., Osher, S. & Miao, J. Accurate real space iterative reconstruction (RESIRE) algorithm for tomography. *Sci. Rep.* **13,** 5624 (2023).